Study of Some of the Nonlinear Effects Produced by Giant Pulse Ruby Laser

Balbhadra Kumar

Department of Physics
BIRLA INSTITUTE OF TECHNOLOGY AND SCIENCE
PILANI (Rajasthan) INDIA
1973

STUDY OF SOME OF THE NONLINEAR EFFECTS PRODUCED BY GIANT PULSE RUBY LASER

THESIS

SUBMITTED IN PARTIAL FULFILMENT

OF THE REQUIREMENT FOR THE

DEGREE OF DOCTOR OF

PHILOSOPHY

by

BALBHADRA KUMAR

At the

BIRLA INSTITUTE OF TECHNOLOGY AND SCIENCE,

PILANI (RAJASTHAN)

1973

Dedicated to my parents

Certified that the work presented in this thesis is original and has been done by Mr. Balbhadra Kumar under my supervision and has not been submitted elsewhere for a degree.

(T.S. Jaseja) 6/9/73
Professor of Physics

Birla Institute of Technology
and Science, PILANI (Rajasthan)

ACKNOWLEDGEMENTS

I would like to express my deep sense of gratitude to Professor T.S. Jaseja for his guidance and constant encouragement throughout the course of present work.

I am very much grateful to Dr. Ved Parkash for the experimental assistance offered by him. I am thankful to the Dean, Faculty of Science for his encouragement in carrying out the present work. I am also grateful to Dr. Mahendra Kumar Dheer, Dr. A.D. Taneja, Shri P.C. Pande and Shri Jai Paul Dudeja for their cooperation and assistance in various ways. I acknowledge the financial assistance in the form of JRF from C.S.I.R.

With BITS-MIT Ford Foundation Programme's support it has been possible to develop the laser-maser research laboratory at B.I.T.S. under the leadership of Dr. T.S. Jaseja. I am, therefore, thankful to all the persons concerned with the programme.

My deepest appreciation is reserved for wife and my parents without their patience and understanding the research could not have been accomplished.

Balbhadra Kumar

TABLE OF CONTENTS

LIST OF TABLES

LIST OF FIGURES

SYNOPSIS

The studies of some of the nonlinear effects produced by Giant pulse ruby laser were made and are reported in this thesis.

Chapter I briefly outlines the higher-order radiation processes produced in a medium when the medium is illuminated with high intense monochromatic electromagnetic wave (laser beam).

Brief account of setting up of various Q-switching devices used in our laboratory is given in Chapter II. A rotating prism device used as one of the Q-switches has been developed here at BITS. The giant ruby laser pulses of power 10-300 Megawatts in a pulse duration 2 or 3×10^{-8} sec. were produced in our laboratory by Q-switching.

Spectroscopic study of fluorescence excited by giant pulse ruby laser in the case of anthracene crystals is reported in Chapter III. The fluorescence spectrum consists of four broad bands in the visible region from blue to violet. The fluorescence is produced by two processes; two-photon absorption process and the process of creation of triplet excitons. The two-photon absorption is explained by 2nd order time-dependent perturbation.

For the first time the spectroscopic study of fluorescence resulted from only two-photon absorption in single crystals of pyrene was carried out and is reported in

Chapter IV.

Spectroscopic study of fluorescence spectrum in visible region resulted from 3-photon absorption in the case of naphthalene single crystal is reported in Chapter V. The 3-photon absorption is explained by 3rd order time-dependent perturbation.

Chapter VI deals with the theory of harmonic generations based on classical mechanics originally developed by Franken and Ward. Nonlinear susceptibilities for second harmonic generations for important crystals quartz, KDP, $LiNbO_3$, Banana and HIO_3 are calculated. Our observations on SHG of 1st order stimulated Stokes radiations produced from CH_3OH and 1,2 dichloroethane are reported in the Chapter VI.

Our experimental observations to determine the spread of 1st order stimulated Stokes radiations are reported in Chapter VII. It was found that the intensity of the 1st order Stokes radiation is well spread and thus is responsible for the high gain observed at 1st order anti-Stokes frequency. The Chapter VII also outlines the theory of SRE based on classical arguments as originally developed by Townes and his coworkers.

++++++++

CHAPTER I

INTRODUCTION

When a light wave propagates through a medium, an interaction of the radiation and the matter takes place. Ordinary light sources produce radiation fields much smaller than the atomic or molecular fields ($\sim 10^8$ V/cm) inside the medium. But when the medium is illuminated with high intense monochromatic light source obtainable from lasers, the interaction of the radiation and the matter via multiple quantum transitions, takes place. In principle, there is no such thing as a transparent substance if one considers higher order radiation processes which become predominant when the radiation fields become comparable to the atomic or molecular fields.

A high intensity light beam may be attenuated, for example, by double-photon absorption if the photon frequency is half that the separation of the two energy levels with the same parity. On the other hand, Raman scattering may occur in which a photon is absorbed with the simultaneous emission of a photon of different energy. As is well known, the Raman process does not require that the pumping light be in resonance with the pump transition. In these radiation processes, the final state of the atomic system is different from that of its initial state.

However, transparent substances acting as non-linear dielectrics may generate light harmonics by absorbing two-photons and simultaneously emitting the sum photon. In this case, the atomic system is left in its initial state, the ground state, a type of process which is a characteristic of parametric interactions. A number of the nonlinear processes are schematically illustrated in Figs. 1 and 2.

MULTIPLE PHOTON ABSORPTION

Two-photon excitation has been observed in the optical region by Kaiser and Garret[1] using the red light, 6943Å, of a ruby optical maser to illuminate $CaF_2:Eu^{2+}$. The observed fluorescence around 4250Å was the indication that the ion was indeed pumped into an excited state by the absorption of two photons from which state it decayed to the fluorescing level. Subsequently, Abella[2] also using the red light from a ruby maser, observed the double photon excitation of the $^6S_{1/2} \longrightarrow {}^9D_{3/2}$ transition in cesium vapour.

Similarly, three-photon absorption was observed by Singh and Bradley[3]. The quantum mechanical picture of the multiple-photon absorption is represented by the schematic energy level diagram shown in Figs. 1a and 1b.

Since a change in the parity is required for an electric dipole transition, double quantum transitions via the electric dipole must occur with no change of parity. Thus, a direct double quantum transition to a level accessible

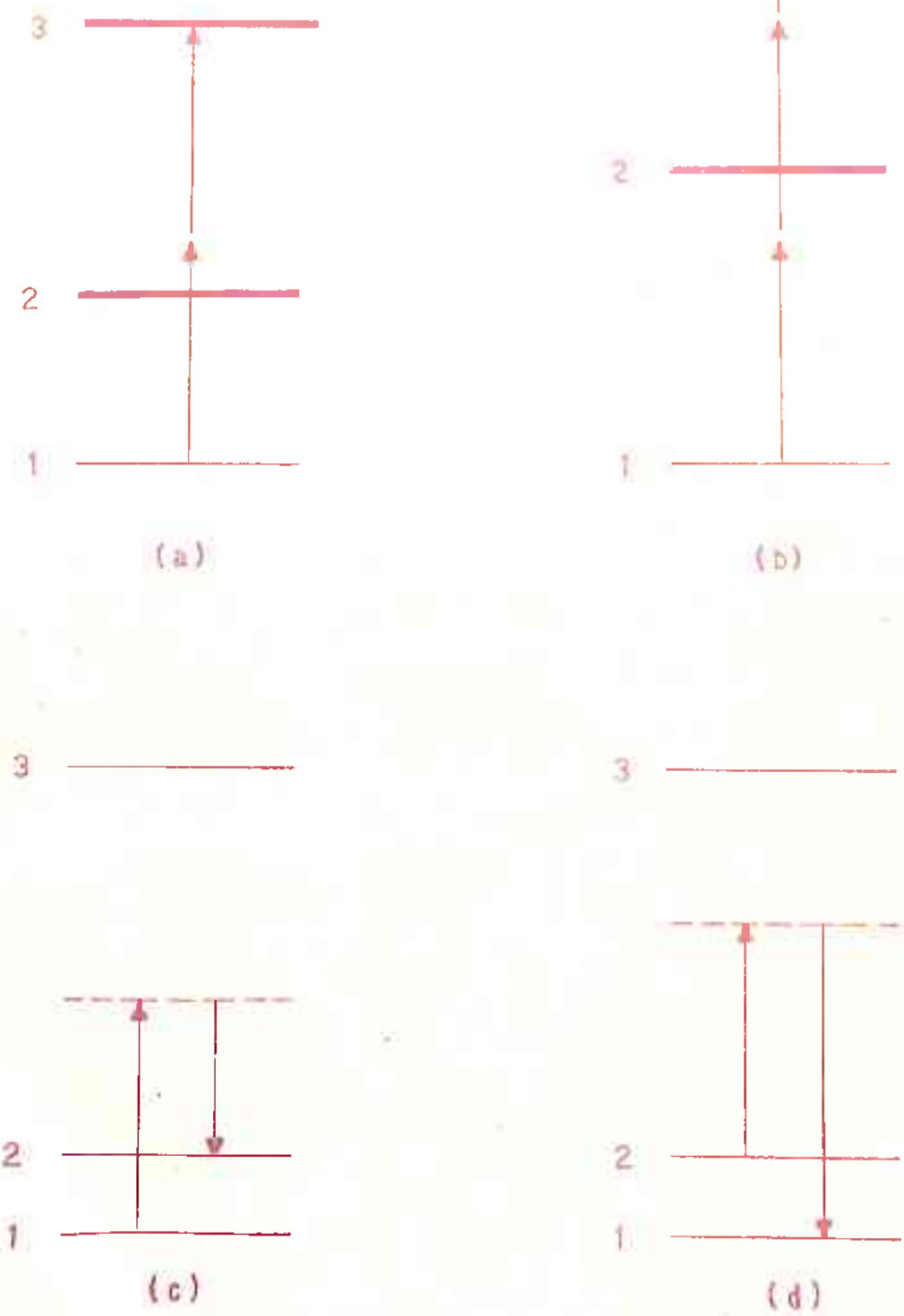

FIG. 1. (a) TWO-PHOTON ABSORPTION; (b) THREE-PHOTON ABSORPTION
(c) RAMAN STOKES EMISSION; (d) RAMAN ANTI-STOKES EMISSION

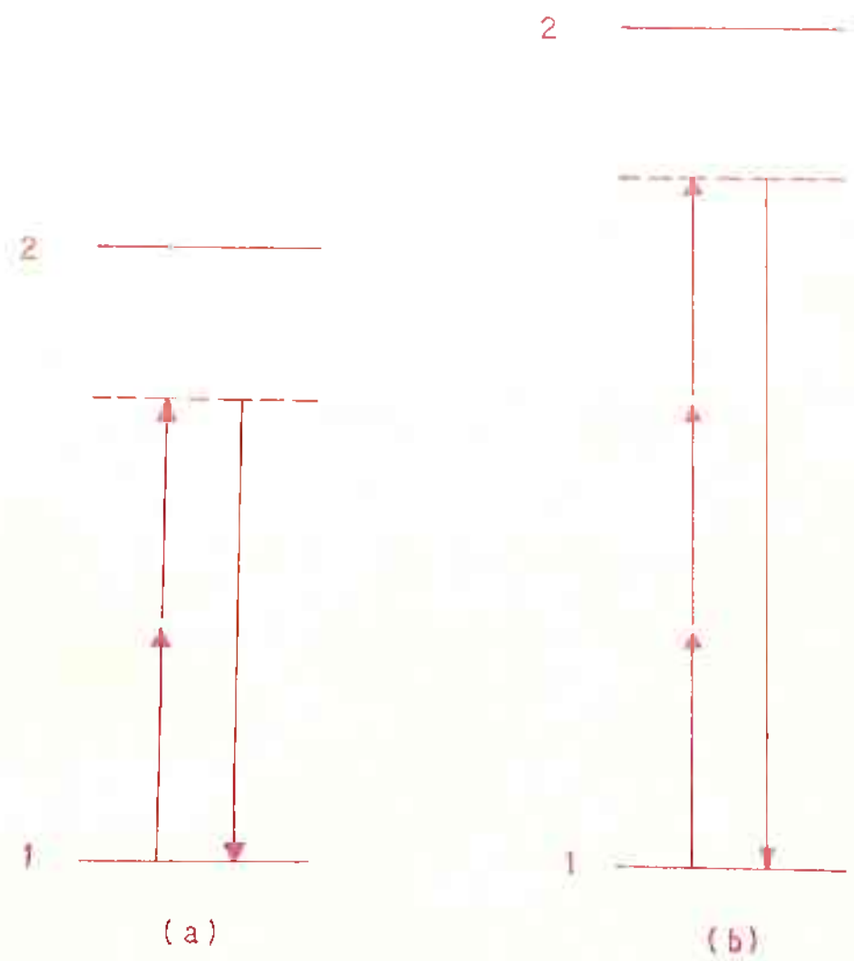

FIG.2 (a) SECOND HARMONIC GENERATION

(b) THIRD HARMONIC GENERATION

by a single quantum transition is forbidden by the parity selection rule for dipole transitions. However, there are atoms in which these selection rules will not be strict and both single and double quantum transitions are possible to the same level by a different component of the dipole operator. The probability that an atom absorbs two photons each of energy $h\nu_p$ has been calculated by Kleinman[4] whose expression for the relevant cross section is

$$\sigma = \left(\frac{e^2}{mc^2}\right)^2 \frac{c^2}{n_a^2 \nu_p^2} FS(2\nu_p - \nu_a).$$

Here, ν_a is the frequency of an absorption band at $\sim 2\nu_p$, $S(2\nu_p - \nu_a)$ is the normalized shape factor of this band, F is the incident flux in photons/cm^2 sec. and n_a is the refractive index at ν_a.

RAMAN EMISSIONS

In these processes, the frequency of the scattered photon is altered. The frequency shift of the scattered photon is the characteristic of the scattering material.

Raman scattering is the inelastic scattering of light by molecules in which the internal energy of the molecule is altered. The quantum mechanical picture of the Raman effect is represented by the schematic energy level diagram shown in Figs. 1c and 1d. The Raman effect is well-known and is easily obtainable by ordinary light source of moderate intensity. In this case, the light is scattered

spontaneously. However, the field supplied by the "giant pulse" laser is very intense and can produce not only spontaneous Raman emission but also induced or stimulated Raman emission (SRE). The details of the SRE are given in Chapter VII.

OPTICAL HARMONIC GENERATION

The process of second harmonic generation is schematically illustrated in Fig. 2a. Here, two photons are absorbed with simultaneous emission of the sum photon. If both the photons absorbed have same energy, the emitted photon will have exact double the energy. If the absorbed photons have different energies, then the emitted photon will have exact sum of the energies. This was first experimentally observed by Franken[5] et al.

In the crystals when the second harmonic generation is forbidden or specially weak (see theory in Chapter VI), third harmonic generation (THG) is the next allowed process. This is schematically illustrated in Fig. 2b.

CHAPTER II

SETTING UP OF "GIANT PULSE" RUBY LASER

INTRODUCTION

The idea of "giant pulse" technique was first given by Hellwarth[6] in 1961. It was suggested[6] that materials which can exhibit normal maser action can also be made to emit short pulses of high amplitude by controlling the regeneration action in the maser cavity. The laser substance is pumped while the regeneration is kept very low by putting a shutter inside the cavity thereby storing a superabundance of ions/atoms in the excited state. At the time when the pumping is just over, the regeneration is then suddenly switched on. In this way, a very large power is released in a short duration, known as "giant" laser pulse. Since the quality factor Q of the laser cavity is switched from very low Q (or spoiling of Q) to very high Q, the process is known as Q-switching or Q-spoiling.

This type of experimental technique was first achieved by McClung and Hellwarth[7] in 1962, using an electro-optical shutter (Kerr cell) in ruby laser cavity. The ruby laser pulses of high amplitude were also obtained by Collins and Kisliuk[8], using a mechanical shutter (rotating disc) and by De Maria, Gagosz and Barnard[9] with an ultrasonic-refraction shutter. In India, the first Q-switching device was successfully developed by Jaseja[10] in the end of 1964 at

Indian Institute of Technology, Kanpur, by using a high speed rotating right-angle prism.

At present rotating mirrors and prisms, Pockels or Kerr cells and saturable absorbers are being utilized for Q-switching purposes. The duration of laser pulses produced by Q-switching usually lies in the range of 5-50 n sec. The availability of these "giant pulses" has made possible the experimental investigation of various non-linear effects, for example,

(i) Multiple-photon excitations.
(ii) Harmonic generations and mixing of optical frequencies.
(iii) Stimulated Raman, Brillouin and Rayleigh-wing scattering.
(iv) Optical self-trapping and self-induced transparency.

Q-SWITCHING DEVICES SET UP IN OUR LABORATORY

In our laboratory "giant pulse" ruby laser with three different types of Q-switches was set up. Giant pulses of peak power 10-300 Mega Watts in a pulse duration 2 or 3×10^{-8} sec could be produced. The Q-switches employed were rotating prism device, passive dye and Pockels cell.

(1) ROTATING PRISM DEVICE

The device has been developed and fabricated here in our laboratory. It is very sturdy and economical and is being usually used for all the experiments. The schematic diagram

of the device is shown in Fig. 3. The regeneration in the laser cavity is very high only during the very short time when the rotating right-angle prism is totally reflecting for the path of the light inside the laser cavity. This position of the right-angle prism (shown in the Fig. 3) is synchronized with the instance the pumping of the laser rod is just over.

The right-angle prism of high optical quality was used for Q-switching. The prism was mounted on a high speed synchronous motor rated for 24,000 r.p.m. A photo cell (RCA 925) was used as a pick-up for the light signal from the prism, when it was about 120° off the laser alignment. This signal was then passed through a delay circuit providing variable delay from 1 m sec to 3 m sec. The delayed signal was amplified by a pulse amplifier. This amplified signal was then used as a trigger to the Xenon flash lamp which provides optical pumping in the laser. By the time the pumping is over the prism takes the position of totally reflecting for the path of light inside the cavity as shown in the Fig. 3.

The total length of the optical cavity was ~ 70 cm. The uncoated front surface of the ruby rod at ~18°C was found to be sufficiently reflecting for the laser action. Therefore, no other partially reflecting mirror was used in the cavity. The optical alignment for the Q-switched laser was done with an autocollimator (Davidson Optronics Inc., USA, model D275). The alignment better than 10" of an arc

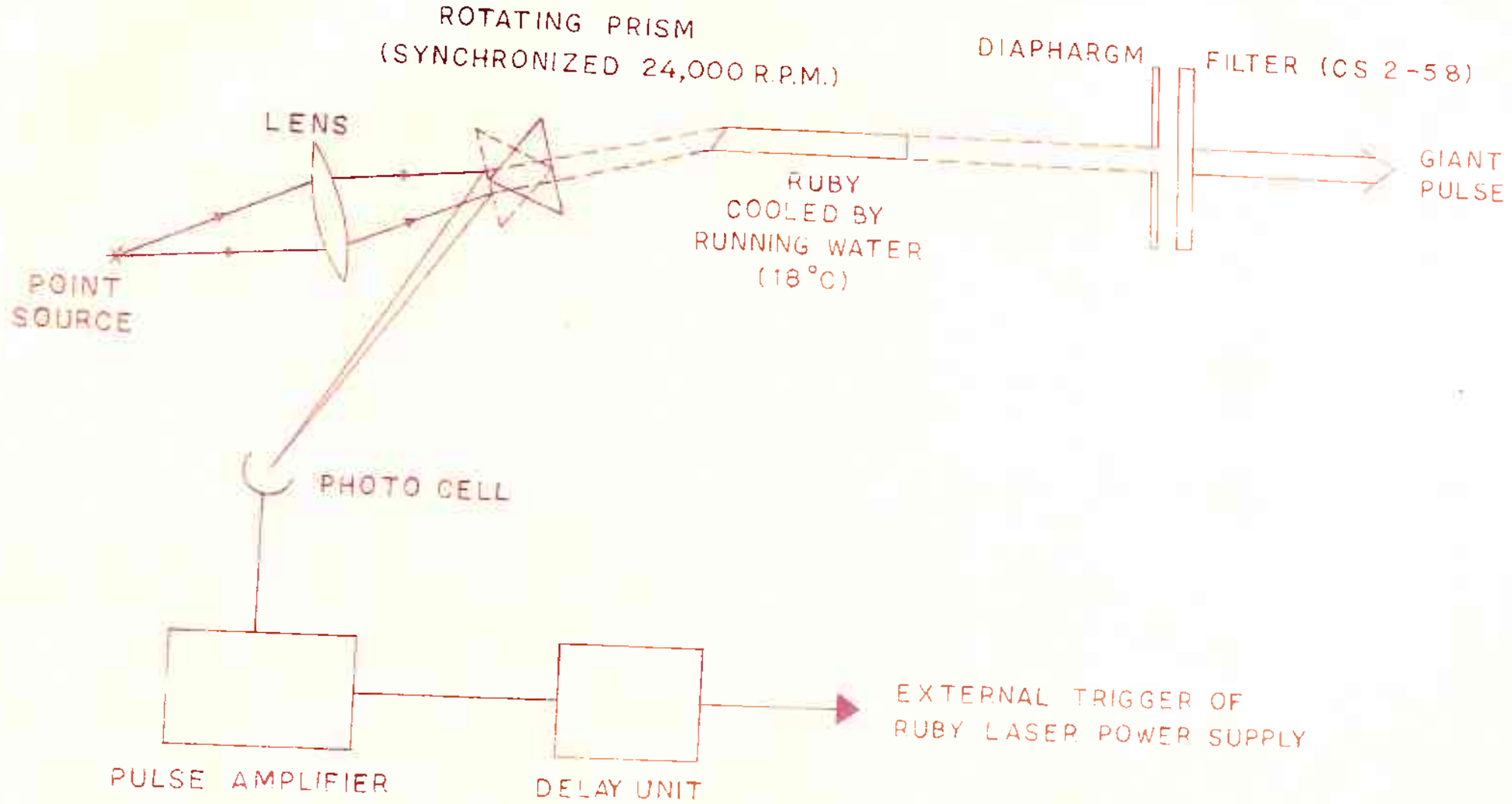

FIG.3 SCHEMATIC DIAGRAM FOR ROTATING PRISM DEVICE USED AS A Q-SWITCH IN THE GIANT PULSE RUBY LASER.

is possible to obtain with this autocollimator.

The pink ruby rod (0.05% concentration of Cr^{3+} ions) of diameter 0.375" and length 6.75" had rough ground lateral surface. One end of the rod was cut at Brewster angle. This end had anti-reflection coating. The temperature of the ruby rod was maintained at 13°C by means of a constant flow of water at the rate of 1-2 gallons per minute. To avoid tarnishing of the laser cavity and to keep the cavity free from moisture, dry nitrogen was passed through the cavity. The ruby was optically pumped by a Xenon flash lamp. The energy to the flash lamp was supplied through a 290 mfd capacity bank, chargeable to the maximum voltage 3 KV DC. The ruby rod, flash lamp and other accessories were housed in a laser head. The laser head and power supply were obtained from Raytheon (USA).

(2) Q-SWITCH PASSIVE DYE

The passive dye (bleachable absorber) is prepared by dissolving 10-20 milligrams of vanadium phtholocyanine (imported from USA) in one litre of monochlorobenzene. The cell with two windows at Brewster angle is filled with this dye and is placed in the laser cavity as shown in Fig. 4.

The dye strongly absorbs light of the ruby frequency and this absorption prevents net amplification of light from occurring until a much larger proportion of Cr^{3+} ions in the ruby material has been pumped to the excited level than is normal. The pumping energy input increases until the

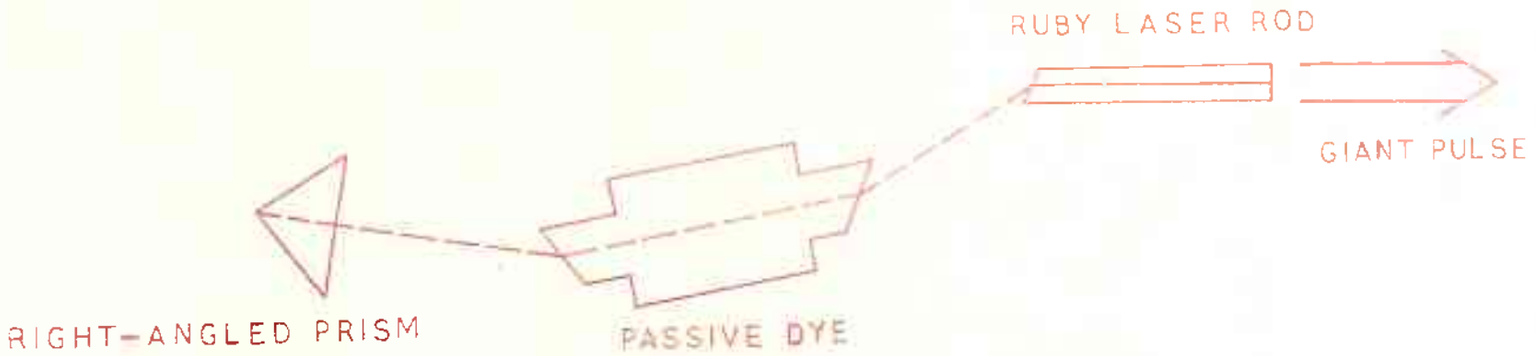

FIG.4 SCHEMATIC DIAGRAM OF PASSIVE Q-SWITCHING.

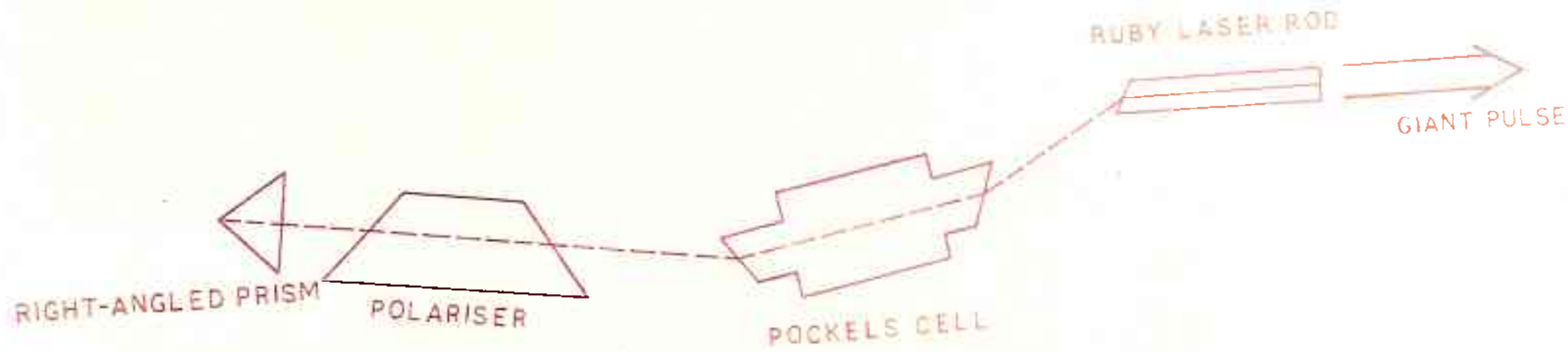

FIG. 5 SCHEMATIC DIAGRAM OF Q-SWITCHING WITH POCKELS CELL.

amplification in the ruby overcomes the loss due to the absorption in the cell, and the laser begins to emit coherent light weakly. A very small amount of this weak laser light "bleaches" the vanadium phthalocyanine solution, which then becomes almost perfectly transparent to the ruby light. At this instant, there is suddenly a large net amplification, and a giant pulse, containing all the stored energy in the ruby, develops rapidly. After the giant pulse, the solution returns quickly to its absorbing state, and becomes ready for the formation of the next giant pulse.

With the passive Q-switching single-mode laser pulses could be produced. For high precision work, the giant pulse ruby laser with this Q-switching is being used e.g. for the study of stimulated Brillouin scattering[11].

(3) POCKELS CELL

When certain kinds of birefringent crystals are placed in an electric field, their indices of refraction are altered by the presence of the field. This effect is known as Pockels effect. This effect is utilized to produce light shutters. The Pockels cell was obtained from Raytheon (USA). The cell is placed in the laser cavity as shown in Fig. 5. The polarized light will pass through the Pockels cell (i.e. regeneration in the cavity) only when the electric field is applied to the cell. In this way, Q-switching is obtained.

All the observations, reported in this thesis, are made with only one single giant ruby laser pulse.

+++++++++

CHAPTER III

FLUORESCENCE SPECTRUM OF ANTHRACENE SINGLE CRYSTALS EXCITED BY GIANT PULSE RUBY LASER

INTRODUCTION

When a substance is illuminated with the intense monochromatic light obtainable from lasers, an interaction of the radiation and the matter takes place via multiple quantum transitions. Such interactions are of two types: one in which the final quantum state of the atomic/molecular system is different from that of its initial state (the ground state), and the other type in which the atomic/molecular system is left in its initial state. The latter type is harmonic generation to be dealt in Chapter VI. The examples of the former are:

(a) Two-photon excitations, in which the light beam may be attenuated by double photon absorption if the photon frequency is one-half of that corresponding to the separation of two energy levels with same parity of the system, is discussed in this chapter and in the Chapter IV. (b) Raman processes, in which a photon is absorbed with simultaneous emission of a photon of different frequency will be discussed in Chapter VII. These processes do not require that the pumping light be in resonance with the pump transition.

The theoretical possibility of two-photon excitation was demonstrated by Göppert-Mayer[12] in 1931, but experimental

realization came only with the advent of lasers because the experiments require a monochromatic source of very high intensity. It was the first experiment of Kaiser and Garret[1] who demonstrated double-photon absorption in CaF_2 crystals doped with Eu.

In the molecular crystals, such as anthracene and pyrene two-photon excitations are expected. Due to these excitations the crystals are expected to fluoresce. It will be interesting to study such fluorescences spectroscopically and to compare the results obtained with those reported earlier, using conventional methods by various earlier workers[13,14].

Different workers[15-19] have studied the fluorescence in anthracene photoelectrically, when excited by a conventional mode operated ruby laser. Peticola et al[15] have reported two-photon absorption as the mechanism for exciting the fluorescence. However, Kepler et al[17] explained the fluorescence by assuming that the laser photons (1.79 ev) directly create triplet excitations (1.8 ev) which, in turn, interact in pairs to form a singlet exciton (3.42 ev) which fluoresces with a life time of 2.6×10^{-8} sec. Lastly, Hall et al[18] suggested that both the mechanisms are capable of producing the fluorescence in anthracene while again studying the fluorescence from anthracene photoelectrically. However, we have actually recorded the fluorescence spectrum in anthracene when excited by giant pulse ruby laser. In this chapter, we are reporting the fluorescence spectrum of anthracene in the

visible region excited by the "giant pulse" ruby laser (6943Å).

In anthracene, the fluorescence spectrum was found to consist of four very broad bands extending from blue to violet.

THEORY

The problem of two-photon absorption* may be treated quantum mechanically, using time-dependent perturbation theory.

We assume a system which, in the absence of a radiation field, has a Hamiltonian H_o and an eigen function ψ_n, where

$$H_o \psi_n = E_n \psi_n. \qquad (3\text{-}1)$$

Here $H_o = \frac{\hbar^2}{2m} \nabla^2 + V(r)$, E_n is the energy of the system and $V(r)$ is the potential energy.

Due to interaction with a radiation field at frequency w, the system is perturbed so that its Hamiltonian becomes

$$H = H_o + H'(t)$$

H_o is the unperturbed Hamiltonian whereas $H'(t)$ is the perturbation. The perturbation matrix elements are written[20] as

$$H'_{km}(t) = \frac{H'_{km}}{2} (e^{iwt} + e^{-iwt}) \qquad (3\text{-}2)$$

We assume that at $t = 0$, the system is in the ground state m of the Hamiltonian. The probability, to the second-order

* when considering a nonlinearity in dielectric constant as $\epsilon = \epsilon_0 + \epsilon_2 E^2$

perturbation, of finding the system at t in the state 1 is given by $\left|a_1^{(2)}(t)\right|^2$ where $a_1^{(2)}(t)$ from the second order time-dependent perturbation theory[20] is given as

$$\dot{a}_1^{(2)}(t) = -\frac{i}{\hbar}\sum_n a_n^{(1)}\, H'_{1n}(t)\, e^{-iw_{n1}t} \qquad (3\text{-}3)$$

Substituting the value of $H'_{1n}(t)$ in the equation (3-3), we get

$$\dot{a}_1^{(2)}(t) = -\frac{i}{2\hbar}\sum_n a_n^{(1)}\, H'_{1n}\left\{e^{i(w-w_{n1})t} + e^{-i(w+w_{n1})t}\right\} \qquad (3\text{-}4)$$

According to the first order time-dependent perturbation theory[20], $a_n^{(1)}$ is given by

$$a_n^{(1)} = -\frac{H'_{nm}}{2\hbar}\left\{\frac{1 - e^{i(w-w_{mn})t'}}{w_{mn} - w} + \frac{1 - e^{-i(w_{mn}+w)t'}}{w_{mn} + w}\right\} \qquad (3\text{-}5)$$

On substitution of the equation (3-5) into the equation (3-4), we get

$$\dot{a}_1^{(2)}(t') = \frac{i}{4\hbar^2}\sum_n H'_{nm}\, H'_{1n}\left\{\frac{1 - e^{i(w-w_{mn})t'}}{w_{mn} - w} + \frac{1 - e^{-i(w_{mn}+w)t'}}{w_{mn} + w}\right\}\times \left\{e^{i(w-w_{n1})t'} + e^{-i(w+w_{n1})t'}\right\} \qquad (3\text{-}6)$$

The integration of the equation (3-6) yields numerous terms. We can limit the number of the terms under consideration by choosing only those terms in which the denominators may be small. Since $w > 0$ and $w_{mn} < 0$, m being the ground state, these are the terms involving $w+w_{mn}$ in the denominator. Thus, the term of interest is

$$a_1^{(2)}(t') = \frac{i}{4\hbar^2} H'_{nm} H'_{ln} \int_0^t \frac{1 - e^{-i(w_{mn}+w)t'}}{w_{mn}+w} e^{-i(w+w_{nl})t'} dt'$$

$$= \frac{1}{4\hbar^2} H'_{nm} H'_{ln} \left\{ \frac{e^{i(w_{ln}-w)t} - 1}{(w_{ln}-w)(w-w_{nm})} + \frac{e^{-i(2w-w_{lm})t} - 1}{(2w-w_{lm})(w-w_{nm})} \right\} \qquad (3\text{-}7)$$

where we used $2w-w_{nm} - w_{ln} = 2w-w_{lm}$.

The resonant absorption results when $2w = w_{lm}$ which corresponds to the second term of the equation (3-7). The squared magnitude of this term is

$$\left| a_1^{(2)}(t) \right|^2 = \frac{\left| H'_{nm} H'_{ln} \right|^2}{16\hbar^4 (w-w_{nm})^2} \frac{\sin^2 \frac{1}{2}(2w-w_{lm})t}{\left[\frac{1}{2}(2w-w_{lm})\right]^2} \qquad (3\text{-}8)$$

The energy level scheme pertinent to the above discussion is shown in the Fig. 6.

We assume that owing to "smearing" of level l, m or both, we can talk only about the probability of finding the difference frequency $(2w-w_{lm})$. This probability per unit w is described by $\rho(2w-w_{lm})$ so that

$$\int_{-\infty}^{+\infty} \rho(x)\, dx = 1 \quad \text{where} \quad x = (2w-w_{lm})$$

The average probability of finding the system at l is thus

$$P(t)_{m\to l} = \frac{1}{16\hbar^4} \frac{\left| H'_{nm} H'_{ln} \right|^2}{(w-w_{nm})^2} \int_{-\infty}^{+\infty} \frac{\sin^2 (\frac{1}{2} xt)}{(x/2)^2} \rho(x)\, dx$$

$$= \frac{1}{8\hbar^4} \frac{\left| H'_{nm} H'_{ln} \right|^2}{(w-w_{nm})^2} \rho(2w = w_{lm})\, \pi\, t \qquad (3\text{-}9)$$

which corresponds to a transition probability rate

$$W_{m\longrightarrow l} = \frac{dP(t)}{dt} = \frac{\pi}{8h^4} \frac{\left|H'_{nm}\, H'_{ln}\right|^2}{(w-w_{nm})^2} \rho\,(2w = w_{lm}) \qquad (3\text{-}10)$$

The equation (3-8) shows that the presence of an energy level n near the mid-point of the energy gap between m and l levels largely enhances the transition m→l (please refer Fig. 6).

If both the matrix elements H'_{nm} and H'_{ln} are of electric dipole type, we have, for an electric field in the x direction,

$$H'_{nm} \sim e\, X_{nm}\, E$$

$$H'_{ln} \sim e\, X_{ln}\, E$$

where E is the amplitude of the electric field. This according to the equation (3-10) gives a transition rate from m to l proportional to E^4, i.e. to the second power of intensity.

It is already shown that for enhancement of two-photon transition, an energy level near the mid-point of m→l transition gap is desirable. The energy level scheme[19] for anthracene single crystal is shown in Fig. 7. In this case a triplet $^3B_{2u}$ state lies at about mid-point between the two singlet levels ^1A_g and $^1B_{2u}$ where two-photon absorption takes place.

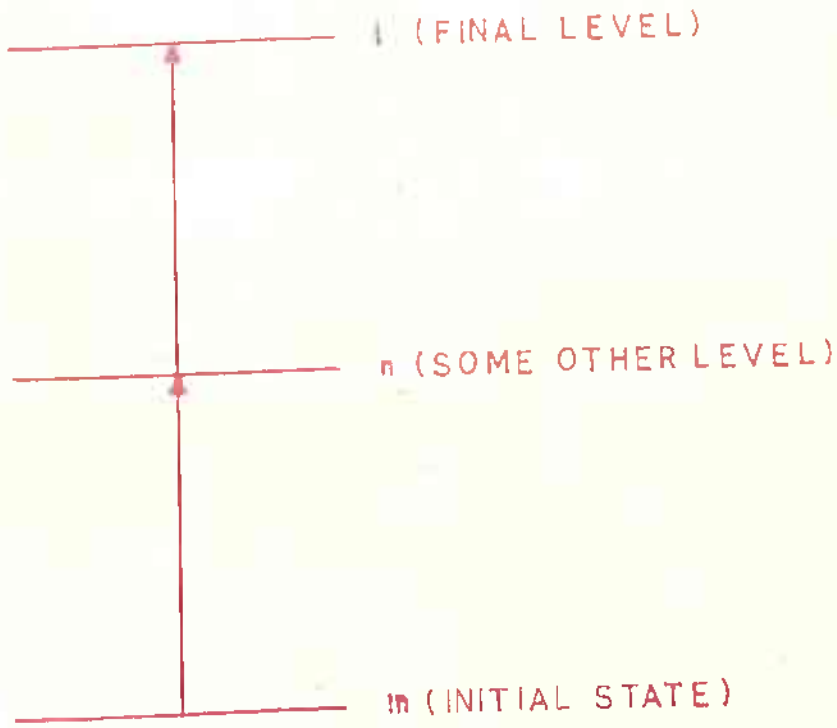

FIG. 6 SHOWS THEORETICAL ENERGY LEVEL SCHEME FOR A SYSTEM IN WHICH TWO-PHOTON ABSORPTION MAY BE ENHANCED.

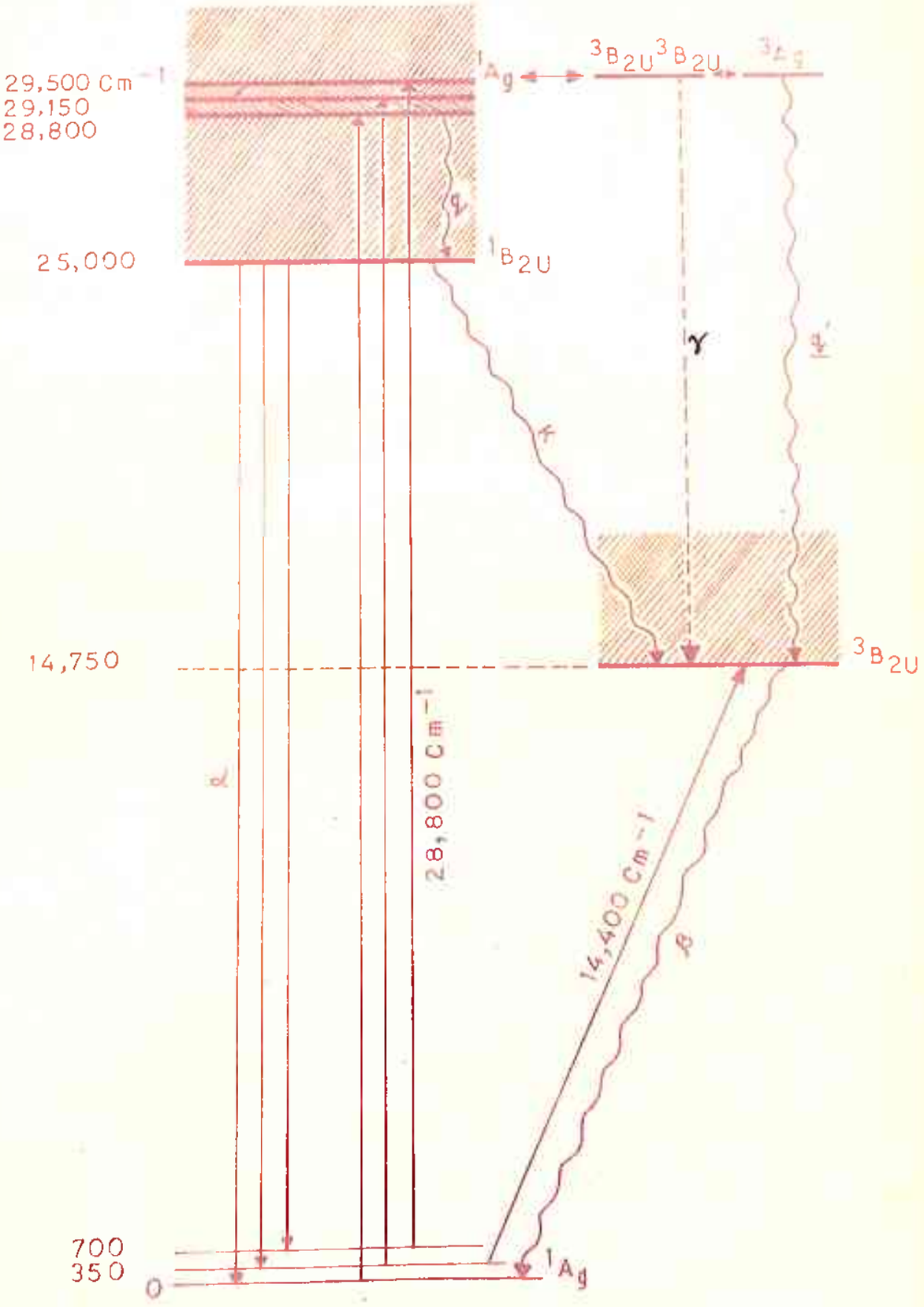

FIG. 7 ENERGY LEVEL DIAGRAM OF ANTHRACENE

EXPERIMENTAL DETAILS

Giant pulses at or near threshold laser operation were used in these experiments. The power near the threshold was about 10-20 MW in a pulse duration $\sim 30 \times 10^{-9}$ sec. The crystals used were thin and pure and they were grown by the slow crystallization from the saturated solutions in absolute alcohol. The crystallization was repeated for three or four times. A Corning glass filter No. Cs 2-58 along with a diaphragm was placed in front of the sample, kept about one-meter away from the laser head, to eliminate Xenon lines (from flash lamp) of wavelengths below 6300 Å. The graph showing transmission percent v/s wavelength for the filter Cs 2-58 is shown in Fig. 8. The crystals under investigation were placed very close to the slit of the spectrograph. A Corning glass filter No. Cs 4-76 was placed at the slit of the spectrograph. The graph showing transmission percent v/s wavelength for this filter Cs 4-76 is shown in the Fig. 9. The spectrograph used was 3-glass prism "Carl Zeiss" spectrograph. The details of the experimental arrangement are given in Fig. 10. Usually in our experiments an unfocussed laser beam near the threshold was used. However, the fluorescence spectra obtained with focussed laser beams were of similar nature as those obtained with unfocussed laser beams. But the laser beam, focussed by a lens of long focal length of 25 cm, near the threshold of the laser operation was capable of producing a quite intense fluorescence spectrum. In these experiments, the laser was always operated near the threshold so that the crystals might not be damaged.

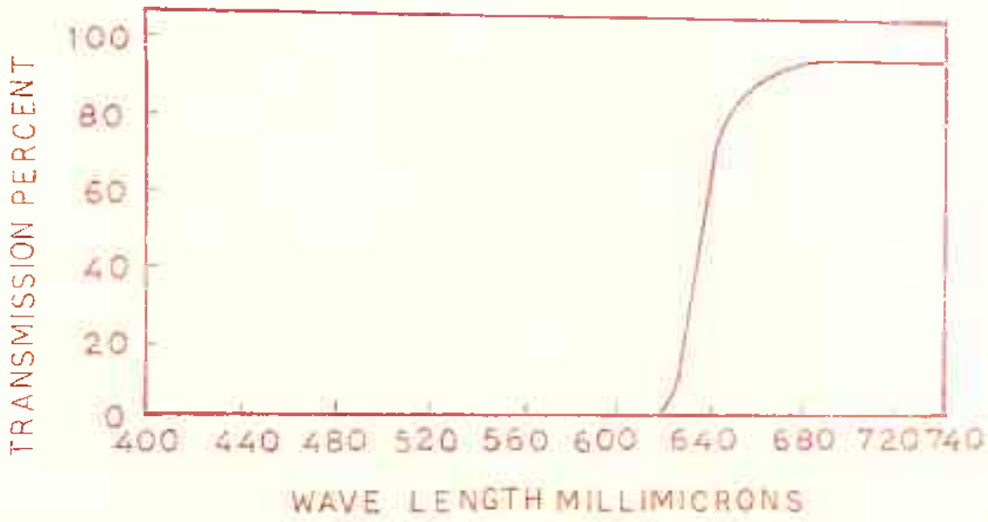

FIG. 8 GRAPH SHOWING TRANSMISSION PERCENT V/S WAVE LENGTH FOR THE FILTER CS 2-58.

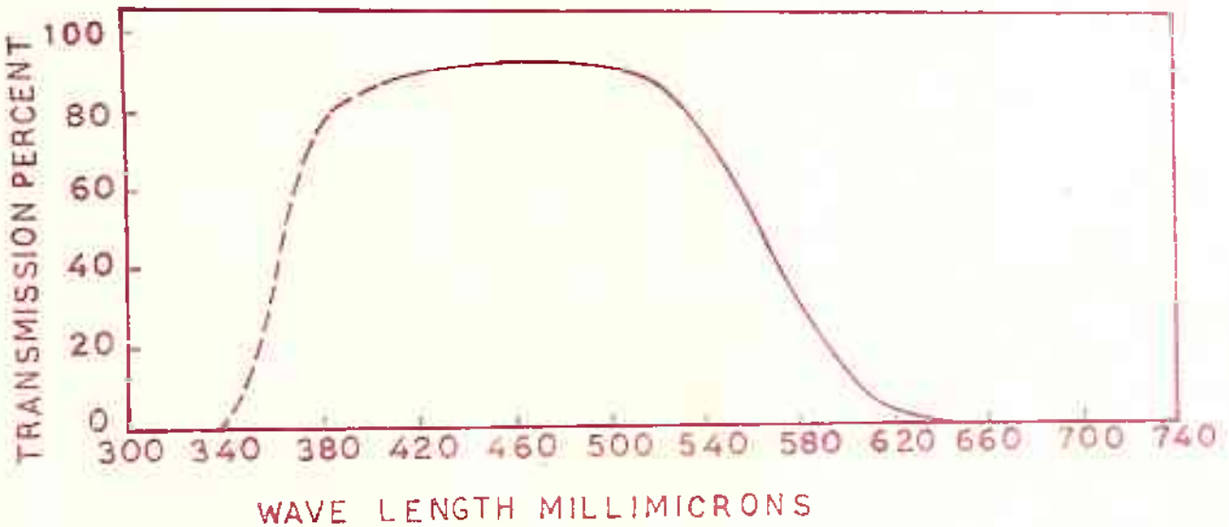

FIG. 9 GRAPH SHOWING TRANSMISSION PERCENT V/S WAVE LENGTH FOR THE FILTER CS 4-76.

FIG. 10 SCHEMATIC EXPERIMENTAL ARRANGEMENT FOR THE STUDY OF FLUORESCENCE SPECTRA RESULTED FROM MULTIPLE-PHOTON ABSORPTIONS.

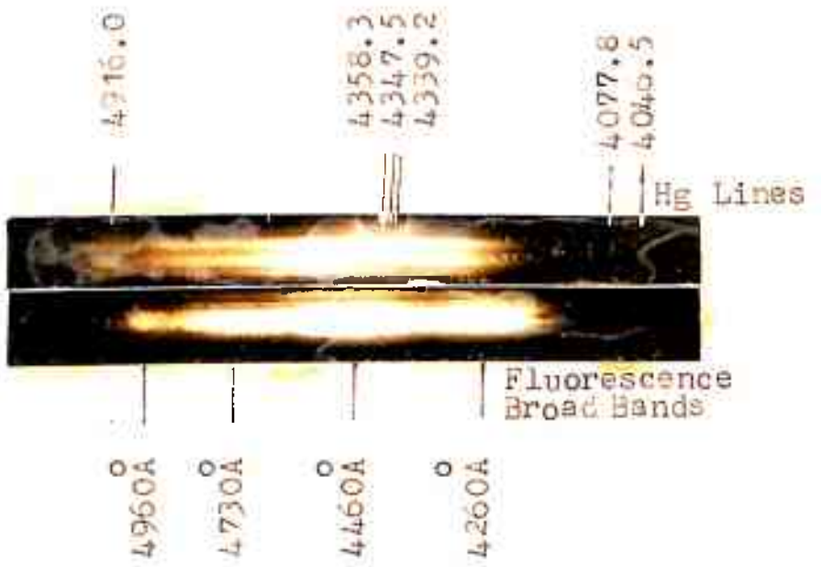

Figure 11. Fluorescence spectrum observed in anthracene when excited by giant-pulse ruby laser near threshold. The lower spectrogram was taken when the input energy for laser operation was increased by 8%.

RESULTS AND DISCUSSIONS

The luminescence spectra of the molecular crystals excited by appropriate intense atomic lines have been of interest to various workers[13,14]. Sidman[21] has reported the fluorescence spectrum of anthracene crystals at 4°K which consisted of three major over-all bands with peaks at around 4040, 4250 and 4520 Å. However, the spectrum of anthracene at room temperature, when excited by giant pulse ruby laser (6943 Å) observed by us consists of four very broad bands. The spectrum is shown in Fig. 11. Each spectrogram, shown in the Fig. 11, was taken with only one laser pulse. The peaks of the bands were found at around 4260, 4460, 4730 and 4960 Å, and the intensities were strong, very strong, strong and medium, respectively.

We have not observed any band near 4000 Å. This may mean that the transition from the fluorescence level to the ground vibrational level at room temperature is not strongly excited when the anthracene molecules are pumped up by ruby laser. On the contrary, we have clearly observed the bands upto 5000 Å. It is, therefore, felt that in our case, the substance may be getting heated up, and thus the excited vibrational levels of the ground electronic state of anthracene may be sufficiently populated. From these excited vibrational levels, the molecules may be pumped up by the laser beam via both the processes[15-18]; the process of two-photon absorption and the process of creating of triplet excitons. Thus, the molecules may efficiently fluoresce to these excited vibrational levels of the ground electronic state.

+++++++++

CHAPTER IV

TWO-PHOTON EXCITATION IN PYRENE SINGLE CRYSTALS

INTRODUCTION

In the case of another molecular crystal, pyrene, the fluorescence spectrum caused by only two-photon absorption process has been investigated by us for the first time. Ferguson[22] and Ganguly and Choudhury[23] have reported the fluorescence spectra of pyrene crystals at 77°K, using conventional sources of light. Their reported fluorescence spectra were continuous extending from 4000 Å to 5600 Å. We have also observed a continuous spectrum extending from green to violet at room temperature when excited by giant pulse ruby laser (frequency 14,400 cm^{-1}).

EXPERIMENTAL DETAILS

Giant laser pulses at or near the threshold laser operation focussed by a lens of focal length 25 cm were used in these experiments. The power near the threshold was about 10-20 MW in a pulse duration $\sim 30\times10^{-9}$ sec. The crystals used were thin and pure and were grown by slow crystallization from saturated solutions in absolute alcohol. The details of the experimental set-up are already given in the Fig. 10 (Chapter III). Each of the spectra was taken with only one single laser pulse.

OBSERVATIONS AND DISCUSSIONS

It is shown in Chapter III that for enhancement of two-photon absorption between levels m and l, an energy level near the mid-point of the transition gap is desirable. The energy level scheme for pyrene[24] crystal is shown in Fig. 12. It is seen in the Fig. 12 that in the case of pyrene also, a triplet level $^3B_{2u}$ lies between the two singlet levels ^1A_g and $^1B_{3u}$ where the two-photon absorption takes place. Thus, the presence of $^3B_{2u}$ level in between ^1A_g and $^1B_{3u}$ may enhance the transition from ^1A_g to $^1B_{3u}$ by two-photon absorption.

Fig. 13 shows the fluorescence spectrum of pyrene when excited by giant pulse ruby laser having frequency 14,400 cm^{-1}. The spectrum shown in the Figure 13 is continuous, extending from violet to green, and is similar in nature as observed by other earlier workers[22,23], using conventional light sources.

In the case of pyrene there may not be the possibility of creating directly the triplet excitons having energy 2.04 ev (16,500 cm^{-1}), since the energy of the laser photons is only 1.79 ev (14,400 cm^{-1}). The singlet excited level $^1B_{3u}$ is situated at 26,500 cm^{-1} and thus the pyrene molecules are pumped up by the laser beam by only two-photon absorption process. From this excited level the molecules decay to fluoresce.

FIG. 12. ENERGY LEVEL DIAGRAM FOR PYRENE

Figure 13. Fluorescence spectrum of pyrene resulted from two-photon absorption

In the case of pyrene, the fluorescence is caused by only two-photon absorption process. This is in contrast to anthracene in which two processes (two-photon absorption process and other, the process of creation of triplet excitons directly) were involved.

+++++:+++

CHAPTER V

FLUORESCENCE SPECTRUM OF NAPHTHALENE CAUSED BY THREE-PHOTON ABSORPTION

INTRODUCTION

In the Chapter III, it is shown that when a proper substance is illuminated with highly intense laser beam, two-photon excitation takes place. Similarly, triple-photon absorption, the higher process than two-photon absorption, results in the generation of fluorescence and is discussed in this chapter. Three-photon excitation has been first observed by Singh and Bradley[3] in the case of naphthalene. They observed the fluorescence caused by three-photon absorption in the ultraviolet region. To the best of our knowledge, no one has observed so far the fluorescence of naphthalene in the visible region. However, we have studied the fluorescence spectrum of naphthalene in the visible region (blue to violet), generated by three-photon absorption. Crystalline naphthalene is a suitable material for observing a three-photon excitation because it has no absorption band system at either ruby laser frequency (14,400 cm^{-1}) or twice the laser frequency. The fluorescence spectrum of naphthalene excited by giant pulse ruby laser observed by us shows sharp bands extending from blue to violet.

THEORY

The three-photon absorption may be explained by third order time-dependent perturbation. The third order coefficient $a_k^{(3)}$ may be given[20] by the expression

$$\dot{a}_k^{(3)} = -\frac{i}{\hbar}\sum a_l^{(2)} H'_{kl}(t')\, e^{iw_{kl}t'} \qquad (5\text{-}1)$$

$$\dot{a}_k^{(3)} = -\frac{i}{2\hbar}\sum a_l^{(2)} H'_{kl}\left\{e^{i(w+w_{kl})t'} + e^{-i(w-w_{kl})t'}\right\}$$

$a_l^{(2)}$ is already derived in Chapter III (equation 3-7).

Substituting $a_l^{(2)}$ in the above equation, we get

$$\dot{a}_k^{(3)} = -\frac{i}{8\hbar^3}\sum H'_{nm} H'_{ln} H'_{kl}\left\{\frac{e^{i(w_{ln}-w)t'}}{(w_{ln}-w)(w-w_{nm})} + \frac{e^{-i(2w-w_{lm})t'}}{(2w-w_{lm})(w-w_{nm})}\right\} \times$$

$$\left\{e^{-i(w-w_{kl})t'} + e^{i(w+w_{kl})t'}\right\} \qquad (5\text{-}2)$$

In the equation (5-2), we are only interested in the second term corresponding to absorption term whose denominator should be small i.e. $2w-w_{lm} \approx 0$ or $\frac{E_l-E_m}{\hbar} \approx 2w$. Therefore

$$a_k^{(3)} = -\frac{i}{8\hbar^3} H'_{nm} H'_{ln} H'_{kl} \int_0^t \frac{\left\{e^{-i(2w-w_{ln})t'} - 1\right\}\left\{e^{i(w+w_{kl})t'} + e^{-i(w-w_{kl})t'}\right\}}{(2w-w_{lm})(w-w_{nm})}$$

$$= -\frac{1}{8\hbar^3}\frac{H'_{nm} H'_{ln} H'_{kl}}{(2w-w_{lm})(w-w_{nm})}\left[\frac{1-e^{-i(w-w_{km})t}}{(w-w_{km})} + \frac{1-e^{i(w+w_{kl})t}}{(w+w_{kl})} + \right.$$

$$\left. + \frac{1-e^{-i(3w-w_{km})t}}{(3w-w_{km})} - \frac{1-e^{-i(w-w_{kl})t}}{(w-w_{kl})}\right]$$

For resonant absorption for three photons i.e. $3w = w_{km}$, we consider only the third term in the above equation, so that

$$a_k^{(3)} = -\frac{1}{8\hbar^3}\frac{H'_{nm}\,H'_{ln}\,H'_{kl}}{(2w-w_{lm})(w-w_{nm})}\frac{1-e^{-i(3w-w_{km})t}}{(3w-w_{km})} \qquad (5\text{-}3)$$

The probability of finding the system in the state k is given by

$$\left|a_k^{(3)}\right|^2 = \frac{1}{64\hbar^6}\frac{\left|H'_{nm}\,H'_{ln}\,H'_{kl}\right|^2}{(2w-w_{lm})^2(w-w_{nm})^2}\left[\frac{1-e^{-i(3w-w_{km})t}}{(3w-w_{km})}\right]\left[\frac{1-e^{i(3w-w_{km})t}}{(3w-w_{km})}\right]$$

On simplification, the above equation yields

$$\left|a_k^{(3)}\right|^2 = \frac{1}{64\hbar^6}\frac{\left|H'_{nm}\,H'_{ln}\,H'_{kl}\right|^2}{\left[(2w-w_{lm})(w-w_{nm})\right]^2}\frac{\sin^2\frac{1}{2}(3w-w_{km})t}{\left[\frac{1}{2}(3w-w_{km})\right]^2} \qquad (5\text{-}4)$$

Since the levels k and m are not precise ones, we can talk only about the probability of finding the difference frequency $(3w-w_{km})$. This probability per unit w is described by $\rho(3w-w_{km})$ so that

$$\int_{-\infty}^{+\infty}\rho(y)\,dy = 1 \qquad \text{where} \quad y = 3w-w_{km}$$

The average probability of finding the system at k is thus

$$P(t)_{m\to k} = \frac{1}{64\hbar^6}\frac{\left|H'_{nm}\,H'_{ln}\,H'_{kl}\right|^2}{\left\{(2w-w_{lm})(w-w_{nm})\right\}^2}\int_{-\infty}^{+\infty}\frac{\sin^2\frac{1}{2}yt}{(y/2)^2}\rho(y)\,dy$$

$$\text{or} \quad P(t)_{m\to k} = \frac{1}{32\hbar^6}\frac{\left|H'_{nm}\,H'_{ln}\,H'_{kl}\right|^2}{\left\{(2w-w_{lm})(w-w_{nm})\right\}^2}\rho(3w=w_{km})\,\pi t$$

which corresponds to a transition probability rate

$$W_{m\to k} = \frac{dP(t)}{dt} = \frac{\pi}{32\hbar^6}\frac{\left|H'_{nm}\,H'_{ln}\,H'_{kl}\right|^2}{\left\{(2w-w_{lm})(w-w_{nm})\right\}^2}\rho(3w=w_{km}) \qquad (5\text{-}5)$$

From the equation (5-4), one would infer that the presence of level l at about two-third of the energy gap between k and m levels and/or the presence of the level n at about one-third of the energy gap between k and m would enhance the transition m→k appreciably as shown in Fig. 14.

For three-photon absorption, naphthalene single crystals were studied. The energy level scheme for naphthalene[3,14] is shown in Fig. 15. The Fig. 15 shows an energy level $^3B_{2u}$, lying in between ^1A_g and $^1B_{3u}$, may help to enhance the transition $^1A_g \rightarrow {}^1B_{3u}$ via three-photon absorption.

EXPERIMENTAL DETAILS

Ruby laser giant pulses of power ~ 50 MW, focussed by a lens of focal length 25 cm, were used to produce the fluorescence spectra of naphthalene. The crystals used were thin and pure, and were grown by slow crystallization from saturated solutions in absolute alcohol. The crystals under investigation were kept about one-meter away from the laser head and were very close to the slit of spectrograph. All the details of experimental arrangement are already given in the Fig. 10 of Chapter III. The unfocussed laser beam of power ~ 100 MW was unable to produce the recordable spectrum. The spectrograph used was 3-glass prism "Carl Zeiss" spectrograph which has sensitivity in the region 4,000Å-10,000Å.

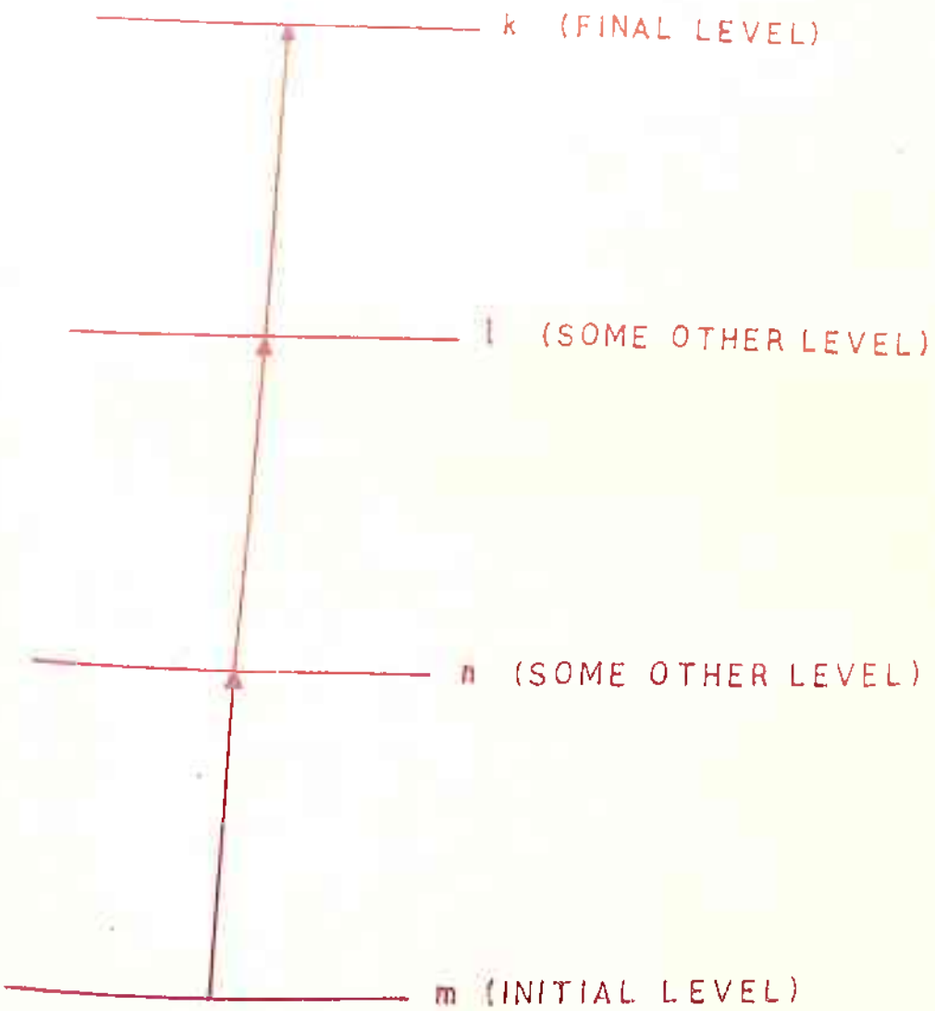

G.14 SHOWS THE THEORETICAL ENERGY LEVEL SCHEME FOR A SYSTEM IN WHICH THREE - PHOTON ABSORPTION MAY BE ENHANCED.

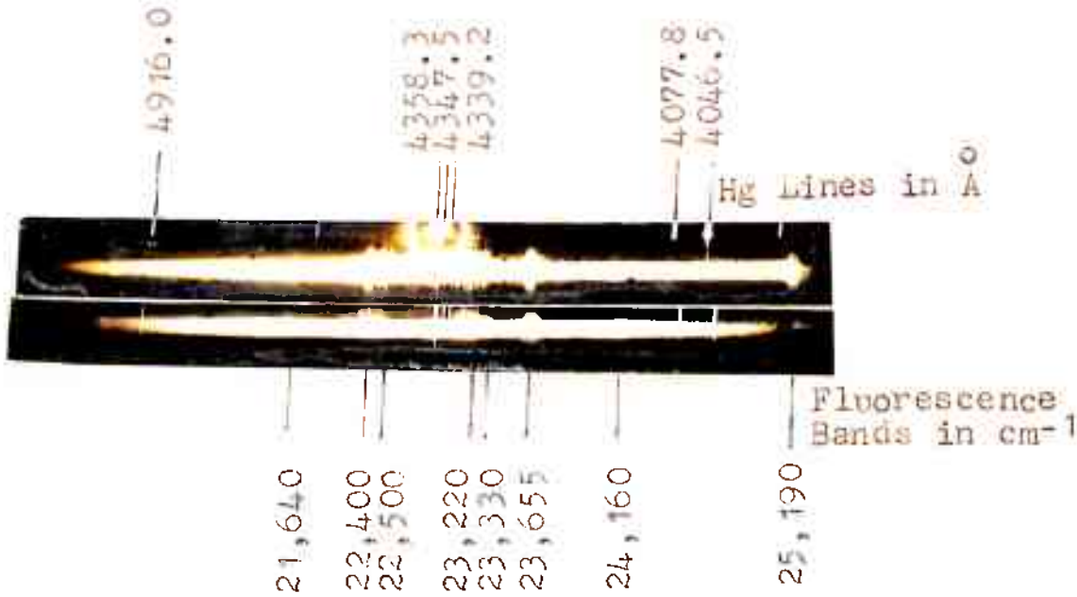

Figure 16. The fluorescence bands of naphthalene in the visible region resulted from three-photon absorption. In the first (top) spectrogram, the slit of the spectrograph was kept 0.1 mm. In the second (bottom) spectrogram, the slit was widened to 0.3 mm.

It has been reported by other earlier workers[14] that the fluorescence origin in the case of naphthalene does not coincide with either of the free exciton absorption components. The fluorescence spectrum is complicated by the presence[14] of the impurity β-methyl-naphthalene and much of the emission from even highly "purified" naphthalene single crystals originates[14] from 31,062 cm^{-1} level of the impurity. The "true" fluorescence origin probably is at 30,950 cm^{-1} and is quite strong at 4.2°K at which temperature the energy transfer[14] to the impurity becomes inhibited. Even this true fluorescence line at 30,950 cm^{-1} observed strongly at 4.2°K is believed[14] to be a vibronic transition from 0-0 band (31,476 cm^{-1}) involving the simultaneous excitation of a ground state vibration 520 cm^{-1} (30,950 ≃ 31,476-520). Therefore, at room temperature, the fluorescence spectrum of naphthalene observed by us is explained by assuming that the transitions are taking place from the level situated at 31,060 cm^{-1} to the excited vibrational levels of the ground electronic state. The observed fluorescence bands are assigned using the vibrational frequencies 518, 1380, 780, 950 and 1020 cm^{-1}. These are listed in the Table 1.

As mentioned earlier in the case of anthracene (Chapter III), the naphthalene single crystals may also be heated up due to strong pumping by high intense laser beam. Thus, the excited vibrational levels of the ground electronic state of naphthalene may be sufficiently populated. From these excited vibrational levels, the molecules may be pumped

by the laser beam via three-photon absorption. Thus, the molecules may efficiently fluoresce to these excited vibrational levels of the ground electronic state.

At 20°K, McClure and Schnepp[25] reported the lattice modes at 96 and 45 cm^{-1}, whereas Obreimov and Shabaldas[26] reported the modes at 103,46 and 15 cm^{-1}. In some of our assignments given in the Table 1, we have used the value of modes as 100 cm^{-1}.

In our experiments to record the spectra of naphthalene in the visible region, laser beam of power density 50 MW/cm^2 focussed by a lens of focal length 25 cm was used. This means that laser photon flux $\sim 10^{28}$ photons cm^{-2} sec^{-1} is required to produce a recordable fluorescence in naphthalene, which is about 10^3 times higher than that required for two-photon excitation in the cases of pyrene and anthracene. However, Singh and Bradley[3] observed the fluorescence in naphthalene in the ultraviolet region with the photon flux $\sim 2\times10^{27}$ photons cm^{-2} sec^{-1}.

TABLE 1. Observed fluorescence bands in naphthalene single crystals along with their possible assignments

S.No.	Observed fluorescence bands (in cm^{-1}) $\pm$ 20 cm^{-1}	Possible assignments (using 0-0 band, ν_0 = 31,062 cm^{-1}) (in cm^{-1})	Calculated frequencies (in cm^{-1})
1	25,190	ν_0 - (2×1380+ 0×518)	25,194
		or	
		ν_0 - (3×1380+ 780 + 950)	25,192
2	24,160	ν_0 - (5×1380)	24,162
		or	
		ν_0 - (2×1380 + 8×518)	24,158
3	23,655	ν_0 - (5×1380 + 518)	23,644
		or	
		ν_0 - (2×1380 + 9×518)	23,640
4	23,330	ν_0 - (3×1380 + 7×518)	23,296
		or	
		ν_0 - (3×1380 + 5×518 + 1020)	23,312

(Contd.)

Table 1 (Contd.)

S.No.	Observed fluorescence bands (in cm^{-1}) $\pm$ 20 cm^{-1}	Possible assignments (using 0-0 band, ν_o = 31,062 cm^{-1}) (in cm^{-1})	Calculated frequencies (in cm^{-1})
5	23,220	ν_o - (3×1380 + 7×518 + 100)	23,196
		or	
		ν_o - (3×1380 + 5×518 + 1020 + 100)	23,212
		or	
		ν_o - (5×1380 + 950)	23,212
6	22,500	ν_o - (4×1380 + 4×518 + 950)	22,520
		or	
		ν_o - (5×1380 + 3×518 + 100)	22,508
7	22,400	ν_o - (4×1380 + 6×518)	22,434
		or	
		ν_o - (4×1380 + 4×518 + 950 + 100)	22,420
8	22,640	ν_o - (5×1380 + 3×518 + 950)	21,658
		or	
		ν_o - (4×1380 + 6×518 + 780)	21,654
		or	
		ν_o - (6×1380 + 2×518 + 100)	21,646

CHAPTER VI

SECOND HARMONIC GENERATION OF STIMULATED STOKES RADIATIONS

INTRODUCTION

With the advent of lasers it is possible these days to produce monochromatic light beams of exceedingly high intensity. For example, the giant pulse ruby laser (6940Å) can provide an optical flux of many MW/cm^2 in an unfocussed beam and many thousands of MW/cm^2 in the focal planes of simple optical system. These intensities make the feasibility of exploiting the optical non-linearities of the materials.

When a substance is illuminated with very intense laser beam, an interaction of the radiation and the matter takes place via multiple quantum transitions. The multiple quantum transitions are expected if one considers higher-order radiation processes. Harmonic generation is one of the processes. The process in which two photons are absorbed with simultaneous emission of the sum photon, is called second harmonic generation (SHG). However, the process in which three photons are absorbed with the simultaneous emission of a photon of triple frequency of the incident photons, is called third harmonic generation (THG). In these harmonic generations, the atomic/molecular system is left in its initial state (refer Fig. 2 in Chapter I).

THEORY

A suitable material for the production of optical harmonics must be relatively transparent to the fundamental optical frequency and the desired harmonics. In addition, there are some important crystal-symmetry considerations which affect the choice of the suitable materials, particularly in the production of even harmonics. The dependence of the optical polarization P as a function of applied intense optical field may be given by scalar expression[5] as

$$P = XE\left(1 + \frac{E}{E_1} + \frac{E^2}{E_2^2} + \ldots.\right) \qquad (6\text{-}01)$$

Here, X is the normal linear optical polarizability and E_1 and E_2 are the atomic/molecular fields of the order of 10^8 e.s.u.

In particular, let us consider the second term of the equation (6-01) which gives rise to the second harmonic. If the applied optical electric field is $E = E_o \cos(wt - \vec{k}.\vec{r})$, then the quadratic term in equation (6-01) provides a contribution 'p' to the polarization in the crystal

$$p = \frac{X}{E_1} E_o^2 \cos^2(wt - \vec{k}.\vec{r}) = \frac{X}{2E_1} E_o^2 \left(1 + \cos(2wt - 2\vec{k}.\vec{r})\right) \qquad (6\text{-}02)$$

Here, first term corresponds to dc polarization within the crystal which arises from the quadratic non-linearity in much the same way as dc currents are produced in the square-law detectors of radio-frequency practice. The second term

in the equation (6-02) is responsible for the radiation of the second harmonic from the crystal.

There does exist a most important symmetry consideration which precludes significantly even harmonic production by the materials which are either isotropic (such as glasses) or possess a centre of inversion (such as calcite). When isotropy or a centre of inversion is present, the polarization must reverse sign for a reversal of applied electric field. In order to comply with this restriction, the terms containing even powers of E in the scalar expression (6-01) must vanish.

A pictorial demonstration of symmetry restriction is indicated in Figs. 17a, b. In the Fig. 17a the polarization dependence of a material is sketched which possesses a centre of inversion. However, the one feature that follows from the symmetry property is that a power expansion of P about $E = 0$ cannot contain even terms. If we now consider crystals which do not have centre of inversion (such as quartz) then it is possible to have a polarization dependence as shown in the Fig. 17b.

A crystal, whose point symmetry precludes even harmonic productions, can nevertheless be forced to produce the effect upon the application of a strong external dc electric field. This external bias field "slides" the origin of the Fig. 17a over into a region, where an expansion of P about the new origin (dotted axes) now contains some even terms.

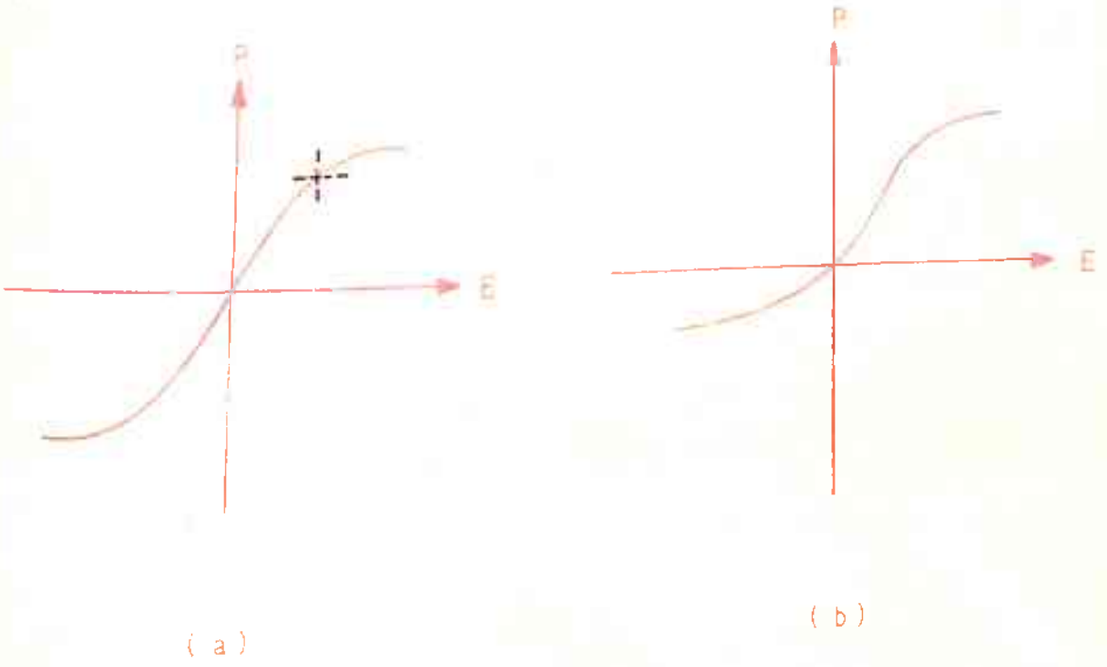

(a) (b)

FIG.17 SCHEMATIC ILLUSTATIONS OF THE DEPENDENCE OF POLARIZATION ON THE APPLIED OPTICAL ELECTRIC FIELD.

(a) IN THE CASE OF CRYSTALS HAVING A CENTRE OF INVERSION.

(b) IN THE CASE OF CRYSTALS WHICH LACK CENTRE OF INVERSION.

SECOND HARMONIC PRODUCTION

The polarization, $p^{2w} \cos 2wt$, corresponding to the SHG, in a nonlinear medium produced by an optical electric field $E^{w} \cos(wt - \vec{k}.\vec{r})$ may be represented by an equation (6-02) in the tensorial form[27] as

$$P_i^{2w} = X_{ijk}^{2w} E_j^{w} E_k^{w} \qquad (6\text{-}03)$$

Here, the summation over repeated indices will be understood even if the summation notation is not employed. Here, subscripts denote cartesian components and the superscripts serve to indicate the relevant frequencies. X^{2w} is a third rank tensor and whose elements X_{ijk}^{2w} are restricted by the symmetry of the non-linear medium.

Consider a particular physical situation described by the equation (6-03). The medium, the applied electric field and the polarization remain fixed in the space and can now be described in a new coordinate frame. The new axes are related to the old by the transformation $\underline{a}$ which can be written as a (3×3) matrix representing an arbitrary combination of rotation and inversion. The vectors and the tensors in the new frame are[27]

$$P_\alpha^{'2w} = a_{\alpha i} P_i^{2w}, \qquad (6\text{-}04a)$$

$$E_\beta^{'w} = a_{\beta j} E_j^{w}, \qquad (6\text{-}04b)$$

$$X_{\alpha\beta\gamma}^{'2w} = a_{\alpha i} a_{\beta j} a_{\gamma k} X_{ijk}^{2w} \qquad (6\text{-}04c)$$

If $\underline{a}$ is now restricted to be a symmetry transformation 'A', then all the properties of the material are identically described in both the coordinate frames. In particular, the elements of the tensor X^{2w}_{ijk} are the same in both the coordinate frames so that[27]

$$X^{2w}_{\alpha\beta\gamma} = A_{\alpha i}\, A_{\beta j}\, A_{\gamma k}\, X^{2w}_{ijk}$$

$$\text{i.e.} \quad X'^{2w}_{\alpha\beta\gamma} = X^{2w}_{\alpha\beta\gamma} \tag{6-05}$$

There are thirty-two classes of the crystals, each specified by a number of point symmetry transformations 'A'. For a particular class, each symmetry transformation yields an equation of the form (6-05) which restricts the independence of the tensor elements $X^{2w}_{\alpha\beta\gamma}$.

As an example of a symmetry restriction, let A be the inversion transformation $A_{\alpha i} = -\delta_{\alpha i}$. The equation (6-05) yields

$$X^{2w}_{\alpha\beta\gamma} = (-\delta_{\alpha i})(-\delta_{\beta j})(-\delta_{\gamma k})\, X^{2w}_{ijk}$$

$$= -\delta_{\alpha i}\, \delta_{\beta j}\, \delta_{\gamma k}\, X^{2w}_{ijk}$$

$$= -X^{2w}_{\alpha\beta\gamma}$$

$$\therefore \quad 2X^{2w}_{\alpha\beta\gamma} = 0$$

$$\therefore \quad X^{2w}_{\alpha\beta\gamma} = 0 \tag{6-06}$$

Since $X^{2w}_{\alpha\beta\gamma}$ is zero, ρ^{2w}_i becomes zero from the equation (6-03). This signifies that X^{2w}_{ijk} is identically zero for any non-linear material showing inversion symmetry and the second harmonic generation is precluded. This leaves for consideration only 21 crystal classes which lack a centre of inversion.

Just like piezoelectricians, we can conveniently replace j and k of X^{2w}_{ijk} by m, taking values 1 through 6 such that $X^{2w}_{im} = X^{2w}_{ijk}$, $j = k$ and $X^{2w}_{im} = X^{2w}_{ijk} + X^{2w}_{ikj}$, $j \neq k$. The relation between m and jk is

m	1	2	3	4	5	6
jk	xx	yy	zz	yz	zx	xy

The non-linear susceptibilities X^{2w}_{ijk} for important crystals have been calculated and are given below:

(I) QUARTZ

In order to calculate X^{2w}_{ijk} we should know A's, the symmetry elements. As it is known, quartz has got D_3 symmetry which has E, C_3, C_3^2, C_a, C_b and C_c elements[28,29]. These elements may be represented in the matrix forms as shown in Appendix 1.

Dropping the superscripts from X in both the sides of the equation (6-05), this equation is rewritten as

$$X_{\alpha\beta\gamma} = A_{\alpha i} \; A_{\beta j} \; A_{\gamma k} \; X_{ijk} \qquad (6\text{-}07)$$

Here, we recall that α, β, and γ vary from 1 to 3 so do i, j and k.

Let $A_{\alpha i}\, A_{\beta j}\, A_{\gamma k}$ be represented by $C_{m,n}$

where

$$m = (\alpha - 1)\, 9 + (\beta - 1)\, 3 + \gamma$$

$$n = (i - 1)\, 9 + (j - 1)\, 3 + k$$

Therefore, the equation (6-07) becomes

$$X_{\alpha\beta\gamma} = \sum_{ijk=1}^{3} C_{m,n}\, X_{ijk} \qquad (6\text{-}08a)$$

The equation (6-08a) can be represented in the matrix form as follows:

$$\begin{bmatrix} X_{111} \\ X_{112} \\ X_{113} \\ X_{121} \\ \vdots \\ X_{333} \end{bmatrix} = \begin{bmatrix} C_{11} & C_{12} & \cdots & C_{1,27} \\ C_{21} & C_{22} & \cdots & C_{2,27} \\ \vdots & \vdots & & \vdots \\ C_{27,1} & C_{27,2} & \cdots & C_{27,27} \end{bmatrix} \begin{bmatrix} X_{111} \\ X_{112} \\ X_{113} \\ \vdots \\ X_{333} \end{bmatrix} \qquad (6\text{-}08b)$$

From the above matrix, the matrix elements can be found by substituting the values of C's which are known by the symmetry of the crystal.

After applying C_3 and C_a symmetry operations, the equation (6-08b) yields matrix elements of the matrix X^{2w}_{ijk} for quartz crystal which are tabulated in the Table (2a). Also, the contracted form of the matrix $X^{2\omega}_{ijk}$ is given in the Table (2b).

(II) KDP (POTASSIUM DIHYDROGEN PHOSPHATE)

KDP crystal has the symmetry D_{2d} or V_d which contains 8 elements; four are pure rotations D_2, two mirror reflections σ_d in two vertical plares and two rotation-reflection S_4 around the principal axis. S_4 is given in the Appendix 1. After applying C_2, S_4 and E (identity) transformations we have calculated from the equation (6-08b) the matrix elements of the matrix X^{2w}_{ijk} which are tabulated in the Table (3a). The contracted form of the matrix X^{2w}_{ijk} is tabulated in Table (3b).

(III) $LiNbO_3$ (LITHIUM NIOBATE)

$LiNbO_3$ belongs to the group C_{3v} which consists of 6 elements E, C_3, C_3^2 and $3\sigma_v$. The elements E, C_3 and σ_v given in the matrix form are shown in the Appendix 1. After applying the transformations C_3 and σ_v', the matrix elements of X^{2w}_{ijk} obtained from the equation (6-08b) are tabulated in the Table (4a). The reduced form of X^{2w}_{ijk} is tabulated in the Table (4b).

(IV) $Ba_2NaNb_5O_{15}$ (BANANA)

The crystal is of symmetry C_{2v} which has elements E, C_2, σ_v and σ_v'. These elements in the matrix form are given in the Appendix 1. Applying the transformations C_2, σ_v, and σ_v', we calculated the matrix elements of X^{2w}_{ijk} from the previous equation (6-08b) and are tabulated in the Table (5a). By symmetry $X_{131} = X_{113}$ and $X_{223} = X_{232}$.

Thus the contracted form of X^{2w}_{ijk} is tabulated in the Table (5b).

(V) HIO_3 (IODIC ACID)

Iodic acid belongs to the group $D_2 \equiv V$ which has the symmetry elements E, C_2, C_a and C_b. These symmetry elements are given in the Appendix 1. Applying the symmetry operations C_2 and C_a, we calculated the matrix elements of X^{2w}_{ijk} from the equation (6-08b) and are given in the Table (6a). By symmetry $X_{123} = X_{132}$, $X_{231} = X_{213}$ and $X_{312} = X_{321}$. Thus, the reduced form of the matrix X^{2w}_{ijk} is tabulated in the Table (6b).

THIRD HARMONIC GENERATION (THG)

The next polarization term p^{3w} cos 3wt after p^{2w} cos 2wt, produced upon the application of extremely intense optical electric field in a non-linear medium, can be expressed in tensorial form[27] as

$$p^{3w}_i = X^{3w}_{ijkl} E^w_j E^w_k E^w_l \qquad (6\text{-}09)$$

Here, the superscripts represent the relevant frequencies and the subscripts denote cartesian components. Despite the omission of the summation sign, the summation over the repeated indices will be understood here and here onwards.

Following exactly the same lines of the treatment for SHG, we can arrive at the following result:

$$X^{3w}_{\alpha\beta\gamma\delta} = A_{\alpha i} A_{\beta j} A_{\gamma k} A_{\delta l} X^{3w}_{ijkl} \qquad (6\text{-}10a)$$

Dropping the superscripts from both the sides of the equation (6-10a), we have

$$X_{\alpha\beta\gamma\delta} = A_{\alpha i}\, A_{\beta j}\, A_{\gamma k}\, A_{\delta l}\, X_{ijkl} \qquad (6\text{-}10b)$$

As we have seen in the case of SHG, the tensors of odd rank are zero for the crystals with centre of symmetry, but here it is not true. Therefore, the crystals with centre of inversion and isotropy can exhibit third-harmonic generation.

Let $A_{\alpha i}\, A_{\beta j}\, A_{\gamma k}\, A_{\delta l}$ be represented by $\rho_{m,n}$

where

$$m = (\alpha - 1)\ 27 + (\beta - 1)\ 9 + (\gamma - 1)\ 3 + \delta$$

$$n = (i - 1)\ 27 + (j - 1)\ 9 + (k - 1)\ 3 + l$$

Therefore, the equation (6-10b) may be represented in the form

$$X_{\alpha\beta\gamma\delta} = \sum_{ijkl=1}^{3} \rho_{m,n}\, X_{ijkl} \qquad (6\text{-}11a)$$

The equation (6-11a) may be written in the matrix form as

$$\begin{bmatrix} X_{1111} \\ X_{1112} \\ X_{1113} \\ X_{1121} \\ X_{1122} \\ X_{1123} \\ X_{1131} \\ X_{1132} \\ \vdots \\ X_{3333} \end{bmatrix} = \begin{bmatrix} \rho_{11} & \rho_{12} & \rho_{13} & \cdots\cdots & \rho_{1,81} \\ \rho_{21} & \rho_{22} & \rho_{23} & \cdots\cdots & \rho_{2,81} \\ \vdots & \vdots & \vdots & & \vdots \\ \rho_{81,1} & \cdots\cdots & \cdots\cdots & \cdots\cdots & \rho_{81,81} \end{bmatrix} \begin{bmatrix} X_{1111} \\ X_{1112} \\ X_{1113} \\ X_{1121} \\ X_{1122} \\ X_{1123} \\ \vdots \\ X_{3333} \end{bmatrix} \qquad (6.11b)$$

The matrix (6-11b) is frequently employed to calculate the non-linear susceptibility coefficients for the crystals whose symmetry elements ρ's are known in the case of THG.

THG was firstly observed by Terhune et al[30] in 1962 in the calcite single crystal, using ruby laser as a pumping source.

EXPERIMENTAL OBSERVATIONS OF SHG

The generation of an optical second harmonic was first observed in the case of quartz single crystal by Franken et al[5] in 1961, using ruby laser as a pumping source. The emergent radiation from the crystal was examined with a prism spectrograph to separate the second harmonic (3470Å) from the enormous amount of laser radiation at 6940Å. It was estimated that $\sim 10^{19}$ incident laser photons produced $\sim 10^{11}$ second harmonic photons, in the interval of ~ 1 msec, characteristic of the laser-pulse.

Second-harmonic generations with unfocussed ruby laser beams were demonstrated by Giordmaine[31] and Maker et al[32] in the case of KDP and quartz. They[31,32] showed the index-matching scheme for KDP for SHG. The total conversion efficiencies of the order of 10^{-6} were achieved by them[31,32] with ruby laser pulses of peak powers of few KW in a pulse duration of $\sim 1/2$ msec when index-matching technique was employed.

Till now various workers[33] have studied SHG using ruby laser or Nd^{+} infrared maser. However, in our experiments the SHG of the stimulated Raman Stokes radiations were produced. From the studies of SHG of the first order stimulated Stokes radiations, the spread of the Stokes radiations was studied. These studies also demonstrated that stimulated Raman emissions (SRE) are produced with sufficient powers and could also be used to produce non-linear effects just like lasers.

In our experiments, ruby laser giant pulses of power ~30 MW in a pulse duration $\sim 30\times10^{-9}$ sec were used to produce stimulated first-order Stokes radiations from CH_3OH (Raman shift 2837 cm^{-1}) and 1,2 dichloroethane (Raman shift 2956 cm^{-1}). These liquids were chosen because of their large Raman shifts so that the Stokes radiations could be easily filtered out. The first order Stokes radiations were produced with sufficient powers ~5 MW.

A Corning glass filter Cs 2-58 was placed before the Raman-cell to eliminate Xenon lines (from the flash lamp used in ruby laser as laser pumping source) of wavelengths below 6300Å. The laser giant pulse was focussed and passed through the Raman-cell (25 cm in length) to produce intense SRE. These SRE were then focussed by a lens of focal length 8 cm onto the front face of KDP single crystal which was aligned in a phase-matched direction[31] for the ruby laser frequency i.e. optic axis at $50^{\circ}\pm1^{\circ}$ from the direction along the thickness dimension. The KDP crystal of thickness 0.5 cm

was highly polished and had parallel faces of size 2 cm × 2 cm. The full experimental arrangement is shown in Fig. 18.

Fig. 19 shows a typical photograph of the focussed SHG of the stimulated first order Stokes radiations generated in CH_3OH. For photographing this focussed SHG, two Corning glass filters No. Cs 5-56 with one Cs 2-58 were placed just after the Raman-cell in order to allow predominantly only first order stimulated Stokes radiation (8643 Å) to pass through KDP single crystal. The graph showing transmission per cent v/s wavelength for the filter Cs 5-56 is shown in Fig. 20. Further, two filters Cs 5-60 were placed just after the KDP crystal for passing only the SHG (4323 Å) of the first order Stokes radiation from the Raman liquid. The graph showing transmission per cent v/s wavelength for this filter Cs 5-60 is shown in the Fig. 21.

The SHG of the first order Stokes radiations generated in CH_3OH and 1,2 dichloroethane were found to be quite intense. The power emitted in SHG is estimated to be $\sim$ 1 KW.

The diameters of such focussed SHG (shown in the Fig. 19) were measured and found to correspond to an angular spread 2 or 3×10^{-2} rad. This may indicate that in forward direction, the intensity of the stimulated first order Stokes radiation is well spread. Further discussion regarding this is given in Chapter VII.

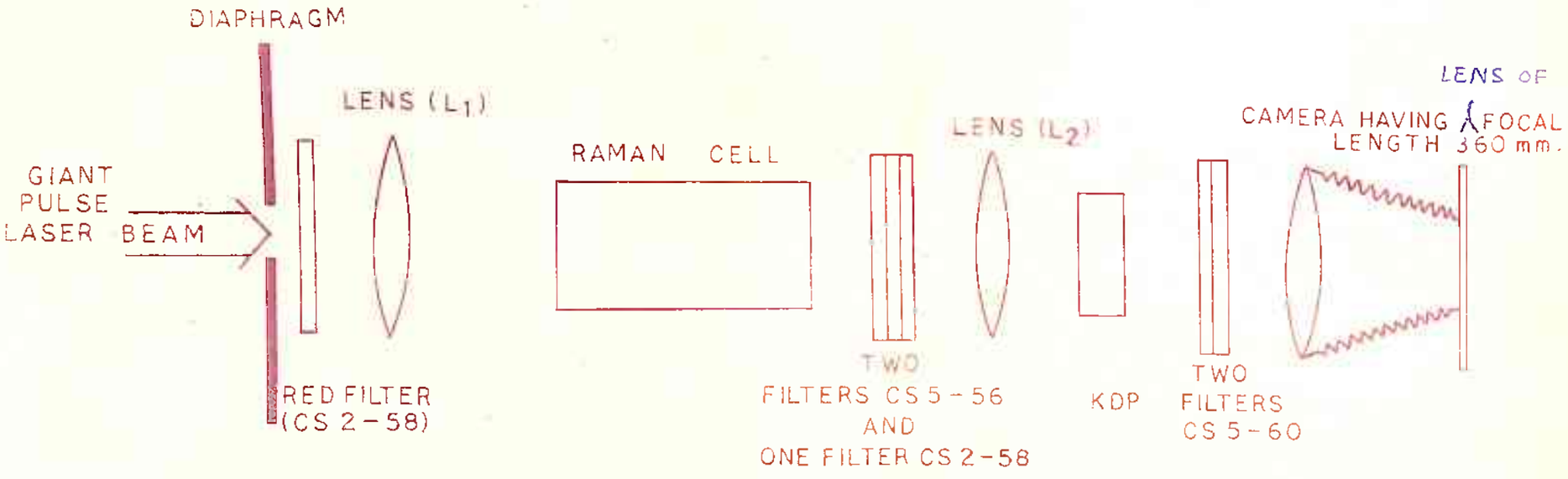

FIG.18 EXPERIMENTAL ARRANGEMENT FOR STUDYING THE SHG OF FIRST ORDER STIMULATED STOKES RADIATIONS.

Figure 19. Typical photograph of focussed SHG of the stimulated first order Stokes radiations

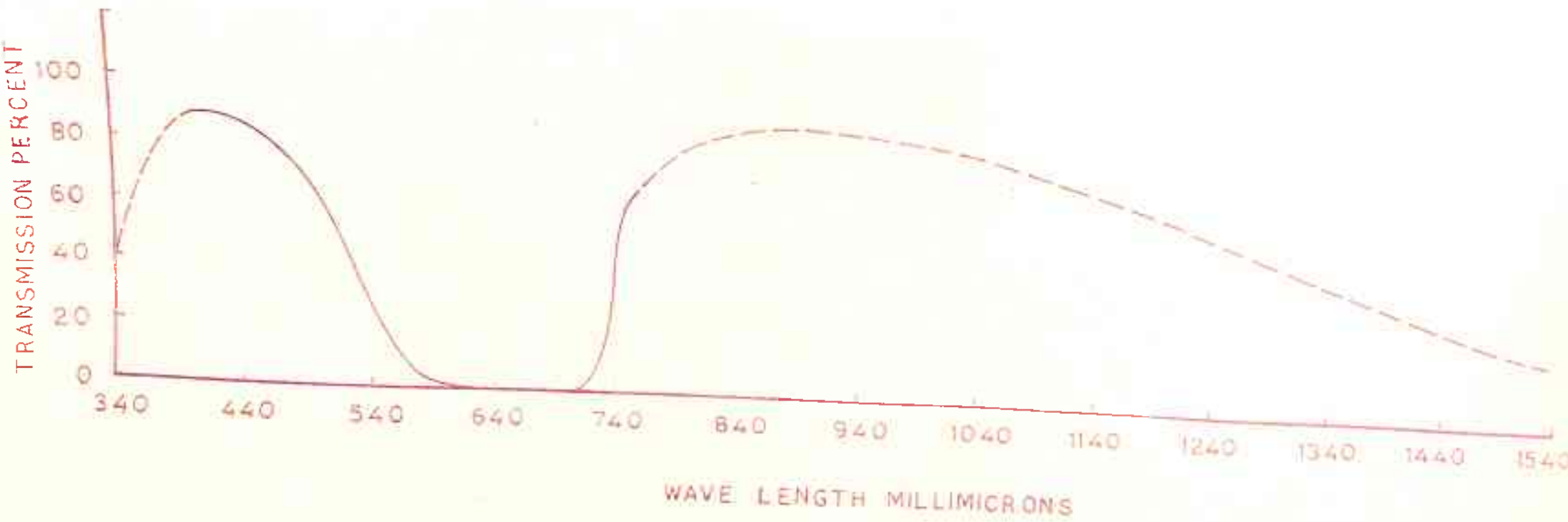

FIG.20 GRAPH SHOWING TRANSMISSION PERCENT V/S WAVE LENGTH FOR THE FILTER CS 5-56.

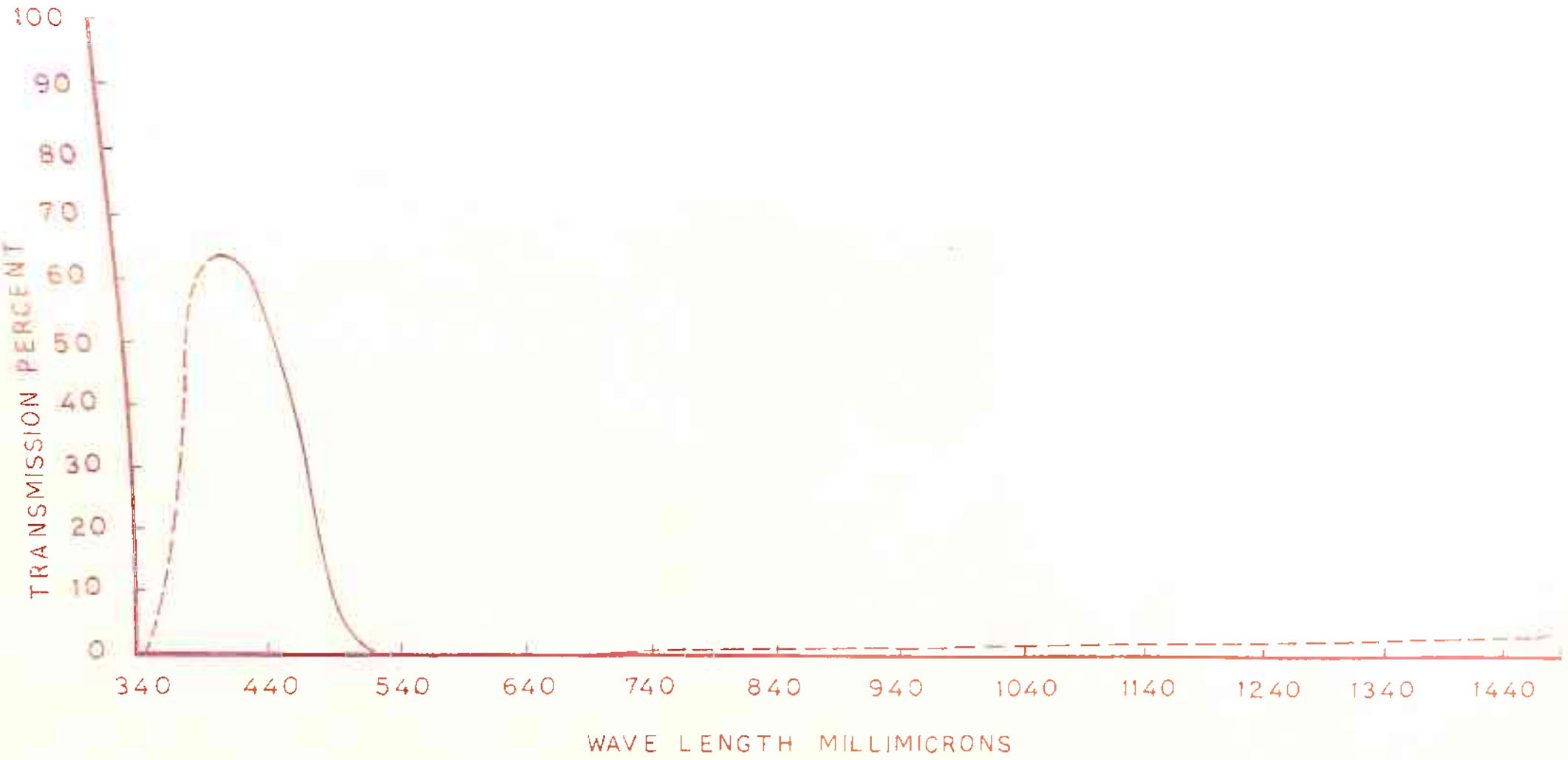

FIG.21 GRAPH SHOWING TRANSMISSION PERCENT V/S WAVE LENGTH FOR THE FILTER CS 5-60.

TABLE 2a The matrix elements of X^{2w}_{ijk} for quartz

i	j	1	2	3	2	3	1	3	1	2
	k	1	2	3	3	1	2	2	3	1
1		e	-e	0	f	0	0	-g	0	0
2		0	0	0	0	g	-e	0	-f	-e
3		0	0	0	0	0	h	0	0	-h

where $X_{111} = e$, $X_{122} = -X_{111} = e$, $X_{123} = -X_{213} = f$
$X_{231} = -X_{132} = g$ and $X_{312} = -X_{321} = h$ and
all other elements of the matrix are zero.

TABLE 2b Contracted form of the matrix X^{2w}_{ijk} for quartz

i	m	1	2	3	4	5	6
1		d_{11}	$-d_{11}$	0	d_{14}	0	0
2		0	0	0	0	$-d_{14}$	$-2d_{11}$
3		0	0	0	0	0	0

Here $m = jk$

$X_{111} = X_{11} = d_{11}$ (say),

$X_{123} = X_{14} = d_{14}$ (say).

TABLE 3(a) The matrix elements of X^{2w}_{ijk} for KDP

i \ j	1	2	3	2	3	1	3	1	2
i \ k	1	2	3	3	1	2	2	3	1
1	0	0	0	a	0	0	b	0	0
2	0	0	0	0	b	0	0	a	0
3	0	0	0	0	0	c	0	0	c

Here $X_{123} = X_{213} = a$,

$X_{231} = X_{132} = b$, and

$X_{312} = X_{321} = c$.

TABLE 3(b) Contracted form of the matrix X^{2w}_{ijk} for KDP

i \ m	1	2	3	4	5	6
1	0	0	0	d_{14}	0	0
2	0	0	0	0	d_{14}	0
3	0	0	0	0	0	0

TABLE 4(a) The matrix elements of X^{2w}_{ijk} for $LiNbO_3$

i \ j k	1 1	2 2	3 3	2 3	3 1	1 2	3 2	1 3	2 1
1	0	0	0	0	a_{15}	a_{16}	0	a_{24}	a_{16}
2	$-a_{22}$	a_{22}	0	a_{24}	0	0	a_{15}	0	0
3	a_{31}	a_{31}	a_{33}	0	0	0	0	0	0

Here $X_{112} = X_{121} = a_{16}$ (say), $X_{113} = X_{223} = a_{24}$ (say)

$X_{131} = X_{232} = a_{15}$, $X_{211} = -X_{222} = -a_{22}$

$X_{311} = X_{322} = a_{31}$, $X_{333} = a_{33}$

By symmetry $X_{131} = X_{113}$ and $X_{223} = X_{232}$

$\therefore a_{15} = a_{24}$

TABLE 4(b) Reduced form of the matrix X^{2w}_{ijk} for $LiNbO_3$

i \ m	1	2	3	4	5	6
1	0	0	0	0	a_{15}	$-a_{22}$
2	$-a_{22}$	a_{22}	0	a_{15}	0	0
3	a_{31}	a_{31}	a_{33}	0	0	0

TABLE 5(a) Matrix elements of X^{2w}_{ijk} for $Ba_2NaNb_5O_{15}$

i \ j	1	2	3	2	3	1	3	1	2
i \ k	1	2	3	3	1	2	2	3	1
1	0	0	0	0	X_{131}	0	0	X_{113}	0
2	0	0	0	X_{223}	0	0	X_{232}	0	0
3	X_{311}	X_{322}	X_{333}	0	0	0	0	0	0

By symmetry $X_{131} = X_{113}$ and $X_{223} = X_{232}$

TABLE 5(b) Contracted form of the matrix X^{2w}_{ijk} for $Ba_2NbNb_5O_{15}$

i \ m	1	2	3	4	5	6
1	0	0	0	0	e_{15}	0
2	0	0	0	e_{24}	0	0
3	e_{31}	e_{32}	e_{33}	0	0	0

Here $X_{131} = X_{113} = e_{15}$, $X_{223} = X_{232} = e_{24}$,
$X_{331} = e_{31}$, $X_{322} = e_{32}$, and
$X_{333} = e_{33}$

TABLE 6(a) Matrix elements of X^{2w}_{ijk} for HIO_3

i \ j k	1 1	2 2	3 3	2 3	3 1	1 2	3 2	1 3	2 1
1	0	0	0	X_{123}	0	0	X_{132}	0	0
2	0	0	0	0	X_{231}	0	0	X_{213}	0
3	0	0	0	0	0	X_{312}	0	0	X_{321}

By symmetry $X_{123} = X_{132}$

$X_{231} = X_{213}$

$X_{312} = X_{321}$

TABLE 6(b) Matrix elements of X^{2w}_{ijk} in reduced form for HIO_3

i \ m	1	2	3	4	5	6
1	0	0	0	e_{14}	0	0
2	0	0	0	0	e_{25}	0
3	0	0	0	0	0	e_{36}

Here $X_{123} = e_{14}$

$X_{231} = e_{25}$

$X_{312} = e_{36}$

CHAPTER VII

SPREAD OF STIMULATED FIRST ORDER RAMAN STOKES RADIATIONS

INTRODUCTION

Stimulated Raman emission (SRE) was discovered by Eckhardt et al[34] who found that when a giant pulse ruby laser beam of sufficient intensity was incident on a Raman cell (filled with nitrobenzene) placed within the laser cavity, stimulated Raman Stokes emissions were emitted. The stimulated Raman scattering differs from the ordinary scattering in the following respects:

(1) it occurs only above a certain intensity threshold of the exciting laser beam,

(2) the output is highly monochromatic especially when the incident laser beam consists of a single frequency,

(3) the efficiency for the generation of SRE is very large 10-20 per cent,

(4) the stimulated Raman radiations are produced in particular directions.

Terhune[35] observed the stimulated Raman emission by focussing the giant pulse laser beam into a Raman-cell kept outside the laser cavity. In this set-up stimulated Raman anti-Stokes as well as Stokes radiations are produced. The stimulated Raman emissions from liquids[35-44], gases[45] and

solids[40] have been studied by several workers.

It is observed that the Raman shifts in the stimulated Raman emission usually belong to totally symmetric mode. The frequency shifts in the second and higher order Raman emissions were observed to be exact multiples of the fundamental Raman shift frequency and not the overtones of the molecular vibrations[36]. It was shown experimentally that the stimulated anti-Stokes and Stokes emissions should be considered as a single process rather than two independent processes[36].

The basic theory of Raman masers was originally given by Javan[47]. The theory for the generation of the stimulated Raman emission has been further developed by several authors[48-51] The first order Stokes wave is produced in the form of diffused radiation when the threshold is reached. The interaction of the intense pump field with the Stokes field causes a variation in the refractive-index[48,49] at the fundamental Raman-shift frequency w_r. The coherent excitation of the molecules responsible for the change in the refractive-index may be treated as modulation present in the medium. This modulation will produce side-bands in the wave scattered by the medium. Thus, the anti-Stokes emission may be produced without further threshold when the incident radiation field and the first order Stokes field are present. The stimulated anti-Stokes waves, generated by the modulation process, will be emitted in a direction determined by the following phase-matching condition for the wave vectors:

$$\vec{K}_o - \vec{K}_{-1} = \vec{K}_n - \vec{K}_{n-1} \qquad (7\text{-}01)$$

where $\vec{K}_o$, $\vec{K}_{-1}$ and $\vec{K}_n$ are the wave vectors associated with the incident (laser) wave, first order Stokes wave and the nth order anti-Stokes wave respectively.

The second and higher order Stokes emissions may also be generated by this modulation process[48,49] and would be emitted in a direction determined by the following phase-matching condition:

$$\vec{K}_o + \vec{K}_{-1} = \vec{K}_{n-1} + \vec{K}_{-n} \qquad (7\text{-}02)$$

where $\vec{K}_{-n}$ is the wave vector associated with the nth order Stokes wave of frequency $(w_o - nw_r)$.

The second and higher order Stokes wave may also be produced by the process mentioned earlier, with a threshold condition. Such Stokes waves will be in the form of diffused radiations.

The stimulated anti-Stokes emission cannot be observed when the Raman-cell is placed inside the laser cavity, because, the phase-matching condition, given by the equation (7-01), could not be satisfied due to dispersion in the medium.

THEORY

Stimulated Raman emission or Raman maser typically involves large number of molecules and photons. Except for the details of molecular characteristics or initiation by

spontaneous emission, these processes may be discussed rather satisfactorily from a classical point of view. As the high intense laser beam passes through the Raman-active medium, spontaneous Raman emission takes place inside the medium. Therefore, we can consider $\vec{E}_o$, the electric field of initial coherent radiation (laser) at frequency w_o and $\vec{E}'$ at frequency $w' = w_o \pm w_r$; w_r being the resonant vibrational frequency of the molecule in the medium.

The total electric field for the travelling waves is

$$\vec{E} = \vec{E}_o \cos(w_o t - \vec{K}_o . \vec{r}) + \vec{E}' \cos(w't - \vec{K}' . \vec{r} + \phi') \qquad (7\text{-}03)$$

where $\vec{r}$ is the position vector for the molecule, $\vec{K}_o$ and $\vec{K}'$ are the propagation vectors corresponding to the radiation fields $\vec{E}_o$ and $\vec{E}'$ respectively. ϕ' is the phase with which the electric field $\vec{E}'$ differs from $\vec{E}_o$.

Let us now consider the vibrating molecule under this electric field $\vec{E}(\vec{r}, t)$, given by the equation (7-03).

The average potential energy of the molecule under the electric field is given by

$$W = -\frac{1}{2}\alpha \left| \vec{E}(\vec{r}, t) \right|^2 \qquad (7\text{-}04)$$

where α is the polarizability.

The polarizability may be expressed upto the first order as

$$\alpha = \alpha_o + \alpha_1 x \qquad (7\text{-}05)$$

Here, x is the deviation from the equilibrium internuclear distance during vibration. α_o is the static polarizability and α_1 is the amplitude of the change in polarizability during vibration. The frequency dependence and tensorial properties of α may be neglected.

The force driving such vibrations is given by

$$F = -\frac{\partial W}{\partial x} = \frac{1}{2}\alpha_1 E^2$$

Substituting the value of E here from equation (7-03), F is written as

$$F = \frac{1}{2}\alpha_1 \left\{ \vec{E}_o^{\,2} \cos^2(w_o t - \vec{K}_o . \vec{r}) + \vec{E}'^2 \cos^2(w't - \vec{K}' . \vec{r} + \phi') + 2\,\vec{E}_o \vec{E}' \cos(w_o t - \vec{K}_o . \vec{r}) \cos(w't - \vec{K}' . \vec{r} + \phi') \right\}$$

Since we are interested only in the terms having w_r, the natural frequency of the molecule, the interested part of the driving force F_{int} is given by

$$F_{int} = \frac{1}{2}\alpha_1 \vec{E}_o \vec{E}' \cos\left\{(w_o - w')t - (\vec{K}_o - \vec{K}') . \vec{r} - \phi'\right\} \qquad (7\text{-}06)$$

Now under this driving force, the differential equation for the vibrating system can be given as

$$m\ddot{x} + R\dot{x} + fx = \frac{1}{2}\alpha_1 \vec{E}_o \vec{E}' \cos\left\{(w_o - w')t - (\vec{K}_o - \vec{K}') . \vec{r} - \phi'\right\} \qquad (7\text{-}07)$$

The solution for x at the frequencies very near to the resonance frequency $w_r = \sqrt{f/m}$ is

$$x = \frac{1}{2}\frac{\alpha_1 \vec{E}_o \vec{E}'}{R(w_o - w')} \sin\left\{(w_o - w')t - (\vec{K}_o - \vec{K}')\,\vec{r} - \phi'\right\} \qquad (7\text{-}08)$$

In the planes defined by $(\vec{K}_o - \vec{K}')\cdot\vec{r} = \text{const.}$, the vibrations of all the molecules are in phase.

The electric dipole moment per unit volume induced by the field $\vec{E}$ is $\vec{\mu} = \alpha \vec{E}$. This oscillating dipole moment may interact with the electric field $\vec{E}' \cos(w't - \vec{K}'\vec{r} + \phi')$ to increase or decrease its amplitude continually, as long as the phase ϕ' is approximately constant. The time averaged rate of energy flow per unit volume to the field $\vec{E}'$ is $N < \frac{d\vec{\mu}}{dt} \cdot \vec{E}' >$. Here, N is the effective number of molecules per unit volume which takes part in the interaction or $N_o - N_1$ where N_o is the density of the molecules in the ground state involved and N_1, the density in the upper state. Hence, the power delivered to $\vec{E}'$ per unit volume is

$$P = \frac{N \alpha_1^2}{8R} \frac{w'}{w_o - w'} (\vec{E}_o \cdot \vec{E}')^2 \qquad (7\text{-}09)$$

The phase ϕ' is arbitrary as long as it does not vary much during the molecular relaxation time $\frac{1}{\Delta w_r}$.

Since the power transferred to $\vec{E}'$ per unit length is quadratic in $\vec{E}'$, there will be a threshold intensity required for $\vec{E}_o$ before the instability takes place, allowing $\vec{E}'$ to build up. For build-up of the travelling wave E', the fractional gain per unit length say 'a' is given as

$$a = \frac{N\pi}{cR} \alpha_1^2 \frac{w'}{w_o - w'} E_o^2$$

For amplification, the gain 'a' must be equal to or greater than the fractional loss per unit length, say 'b' and thereby it leads to the requirement $a \geq b$ i.e.

$$E_o^2 \geq \frac{bcR}{\pi N \alpha_1^2} \frac{w_o - w'}{w'}$$

For the Stokes radiation $w' = w_o - w_r$, so that the condition for Stokes radiation for amplification will be

$$E_o^2 \geq \frac{bcR}{\pi N \alpha_1^2} \frac{w_r}{w_o - w_r} \qquad (7\text{-}10)$$

Once this threshold condition on intensity of the "pump" field E_o is met, the coherent Stokes radiation will increase from the spontaneous Raman emission with the exponential build-up.

ANTI-STOKES GENERATION

The coherent molecular viorations set up by $\vec{E}_o$ and $\vec{E}'$ cause variations in the refractive-index at frequency w_r. Thus, the anti-Stokes radiation at frequency $w_o + w_r$ will be generated, in addition to another type of Stokes wave, a frequency $w_o - w_r$.

To be able to understand in detail the generation of the anti-Stokes radiation, consider the case where electromagnetic waves of both Stokes and anti-Stokes frequencies are initially present, then the total electric field will be

$$\vec{E} = \vec{E}_o \cos(w_o t - \vec{K}_o \cdot \vec{r}) + \vec{E}_{-1} \cos\left\{(w_o - w_r)t - \vec{K}_{-1} \cdot \vec{r} + \phi_{-1}\right\}$$
$$+ \vec{E}_1 \cos\left\{(w_o + w_r)t - \vec{K}_1 \cdot \vec{r} + \phi_1\right\} \qquad (7\text{-}11)$$

As calculated earlier, the average power produced per unit volume at Stokes frequency is

$$P_{-1} = \frac{N\alpha_1^2}{8R}\,\frac{w_o - w_r}{w_r}\left[(\vec{E}_o\,\vec{E}_{-1})^2 + (\vec{E}_o\,\vec{E}_{-1})(\vec{E}_o\,\vec{E}_1)\cos\left\{(2\vec{K}_o - \vec{K}_1 - \vec{K}_{-1})\cdot\vec{r} + \phi_1 + \phi_{-1}\right\}\right] \qquad (7\text{-}12)$$

Similarly, the average power per unit volume at the anti-Stokes frequency is:

$$P_{+1} = \frac{N\alpha_1^2}{8R}\,\frac{w_o + w_r}{w_r}\left[-(\vec{E}_o\,\vec{E}_1)^2 - (\vec{E}_o\,\vec{E}_1)(\vec{E}_o\,\vec{E}_{-1})\cos\left\{(2\vec{K}_o - \vec{K}_1 - \vec{K}_{-1})\cdot\vec{r} + \phi_1 + \phi_{-1}\right\}\right] \qquad (7\text{-}13)$$

From the equation (7-12), it is evident that the Stokes waves will be amplified even in the absence of anti-Stokes wave. However, there is no possibility of achieving power at anti-Stokes wave unless the Stokes radiation is present (refer the equation (7-13)). If $\vec{E}_{-1}$ is zero (Stokes wave absent) the power at the anti-Stokes wave is given as

$$P_{+1} = -(\vec{E}_o\,\vec{E}_1)^2\,\frac{N\alpha_1^2}{8R}\,\frac{w_o + w_r}{w_r} \qquad (7\text{-}14)$$

The equation (7-14) shows that P_{+1} is negative, meaning by no power gain at anti-Stokes wave. From the equation (7-13), it is expected that when $\vec{E}_{-1} > \vec{E}_1$, and if $2\vec{K}_o = \vec{K}_{-1} + \vec{K}_1$ and phase $\phi_1 + \phi_{-1} = \pi$, the maximum power will be emitted at anti-Stokes frequency.

It will be easily seen that the gain at the anti-Stokes wave is not quadratic in E_1 and thus there is no additional threshold needed for its generation beyond the required presence of E_{-1}.

Since there is no condition on the wave vectors from the gain term for the first order Stokes radiation, it will be radiated into all directions, but generally it will build up in the direction of maximum gain, which is parallel to the pump beam. On the other hand, for the gain in the anti-Stokes wave, the wave vector relation

$$2\vec{K}_o = \vec{K}_1 + \vec{K}_{-1} \qquad (7\text{-}15)$$

is required. This relation (7-15) confines the anti-Stokes radiation to a cone in the forward direction, with half angle θ_1, around the initial beam. For small angles the above wave vector relation yields

$$\theta_1^2 \approx \frac{1}{n}\frac{w_o - w_r}{w_o + w_r}(\Delta n_1 - \Delta n_{-1}) + \frac{w_r}{w_o}(\Delta n_1 + \Delta n_{-1}) \qquad (7\text{-}16)$$

Here $n = n(w_o)$ is the index of refraction at frequency w_o.

$$\Delta n_1 = n(w_o + w_r) - n(w_o)$$

and $$\Delta n_{-1} = n(w_o) - n(w_o - w_r)$$

These angles are typically of the order of few degrees.

As was stated above, the presence of E_1 is necessary for the generation of anti-Stokes wave. Thus, it is interesting to study the spread of the first order Stokes radiation

to find whether the spread of the first order Stokes is comparable to the angular spread of the first order anti-Stokes radiation.

EXPERIMENTAL DETAILS

As is seen in the theory, the first order anti-Stokes radiation is produced in a specific direction determined by the wave vector relation

$$\vec{K}_o - \vec{K}_{-1} = \vec{K}_1 - \vec{K}_o$$

And its generation also requires the presence of first order Stokes radiation. Thus, it is expected the first order Stokes radiation will be produced in a well spread region for the generation of intense first order anti-Stokes radiation. To confirm this, an experiment described in this chapter is set up. Our experiment shows that the first order Stokes radiation is well spread to give sufficient power for building up of the first order anti-Stokes radiation.

To demonstrate the spread of the stimulated first order Stokes radiation, it is necessary to filter out the first order Stokes radiations from all SRE and laser radiation. Thus, for this study methyl alcohol (Raman shift 2837 cm^{-1}) and 1,2 dichloroethane (Raman shift 2956 cm^{-1}) were chosen because of their large Raman shifts. Many orders of Stokes radiations as well as anti-Stokes radiations are readily produced. Since all the Stokes radiations fall in the infrared region, it was not possible to filter out completely the first order Stokes radiation alone from other

higher order Stokes lines as well as from strong Xenon lines (from flash lamp) in the infrared region with the available filters in our laboratory. The second and higher order Stokes lines are also produced as cones of radiations. Therefore, it could not be possible to study the spread of the first order Stokes radiation by directly photographing it. Thus, the SHG of the first order Stokes radiations was studied. The spread observed in the SHG may be less than the actual spread of the first order Stokes radiation but would not be much different from the actual spread when the non-linear material (KDP crystal) used for the SHG is employed in the phase-matched direction[31]. The details of the experimental set-up are already given in Chapter VI (see Fig. 18) for photographing of the SHG of first order Stokes radiations generated from methyl alcohol and 1,2 dichloro-ethane.

However, to record the stimulated Raman spectra, 3-glass prism "Carl Zeiss" spectrograph was used which is sensitive in the region 4,000-10,000Å. The schematic diagram for the experimental arrangement for recording the spectra is shown in Fig. 22.

RESULTS AND DISCUSSIONS

Stimulated Raman spectra of CH_3OH and 1,2 dichloro-ethane showing first order Stokes radiations are shown in the Figures 23 and 24.

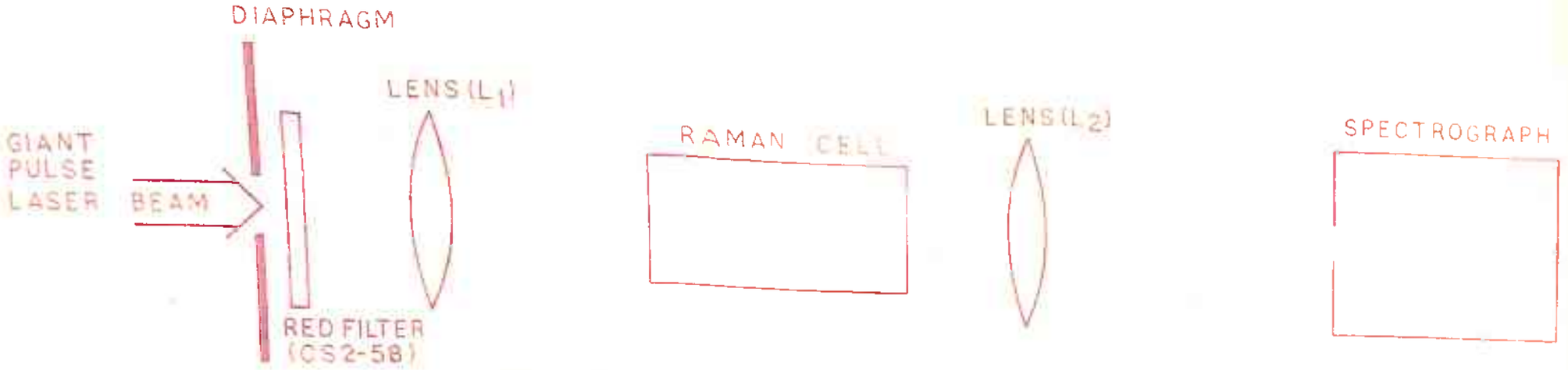

FIG.22 SCHEMATIC EXPERIMENTAL ARRANGEMENT FOR RECORDING STIMULATED RAMAN SPECTRA.

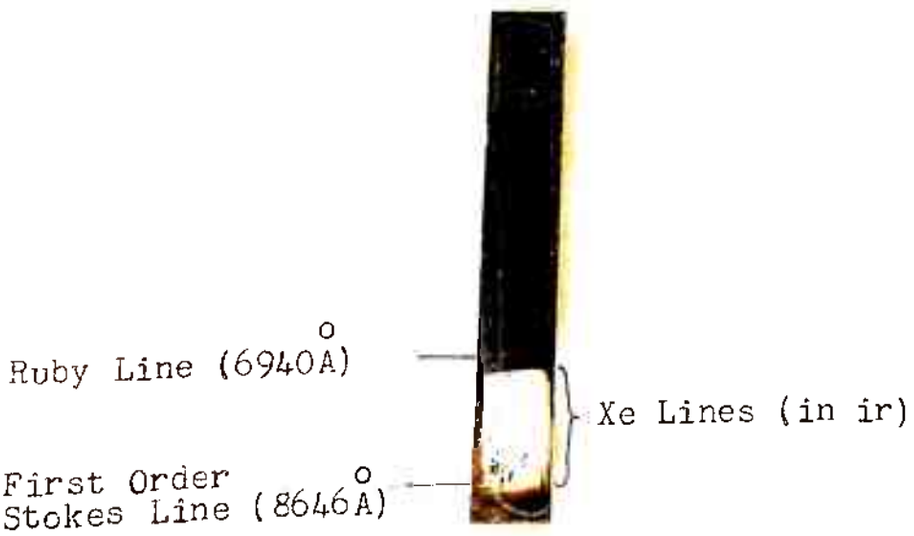

Figure 23. The stimulated Raman spectrum showing first order Stokes line in the case of CH_3OH

A typical focussed SHG of the first order Stokes radiation from CH_3OH is shown in the Fig. 19 (Chapter VI). For photographing the SHG of the first order Stokes radiations, suitable Corning glass filters were used just after the Raman cell in order to eliminate the laser radiation and all the anti-Stokes emissions before KDP crystal. Further, proper filters for passing only the SHG of the first order Stokes radiations, were also placed just after KDP crystal. These details are already given in Chapter VI.

The diameters of the focussed SHG of the first order Stokes radiations (shown in the Fig. 19, Chapter VI) were measured and found to correspond to an angular spread of 2 or 3×10^{-2} rad. This indicates that in the forward direction, the intensity of the first order Stokes radiation is well spread. The emission angle of the first order anti-Stokes radiation obtained from the linear phase-matched (equation (7-15)) is approximately 4×10^{-2} rad. Therefore, the presence of such an intense first order Stokes radiation in this well-spread region is responsible for the high gain observed[39,52] at first-order anti-Stokes frequency. Thus, our experiments confirm this aspect of the theory.

The SHG of the first order Stokes radiations were found to be quite intense (power emitted > 1 KW). This demonstrates also that the Stokes radiations are produced with very large powers[39,52]. Therefore, the Raman masers could also be used as laser radiations to produce various non-linear effects[39].

++++++++++

APPENDIX 1

Let us consider two rectangular axes X and Y and third z-axis at right angles to both X and Y axes, and perpendicular to the plane of paper. In this three-dimensional space the point P is labelled as (x,y,z), and (x',y',z') when x and y axes are rotated about z-axis through an angle θ.

From the Figure 25, we can write

$$\begin{aligned} x &= x' \cos\theta - y' \sin\theta + z'.0 \\ y &= x' \sin\theta + y' \cos\theta + z'.0 \\ z &= x'.0 + y'.0 + z'.1 \end{aligned} \qquad (1)$$

The equation can be given in a matrix form as

$$\begin{bmatrix} x \\ y \\ z \end{bmatrix} = \begin{bmatrix} \cos\theta & -\sin\theta & 0 \\ \sin\theta & \cos\theta & 0 \\ 0 & 0 & 1 \end{bmatrix} \begin{bmatrix} x' \\ y' \\ z' \end{bmatrix} \qquad (2)$$

In the group theory the first matrix on the right hand side is known as matrix for a rotation of angle θ about z-axis. Similarly, the matrices for rotation about x and y axes can be written.

According to group theory if a body is brought imto coincidence with itself after a rotation through an angle $\psi = \frac{2\pi}{n}$ (n integral) about a certain axis, such axis is called n-fold rotation axis. If $n = 1$, we have coincidence

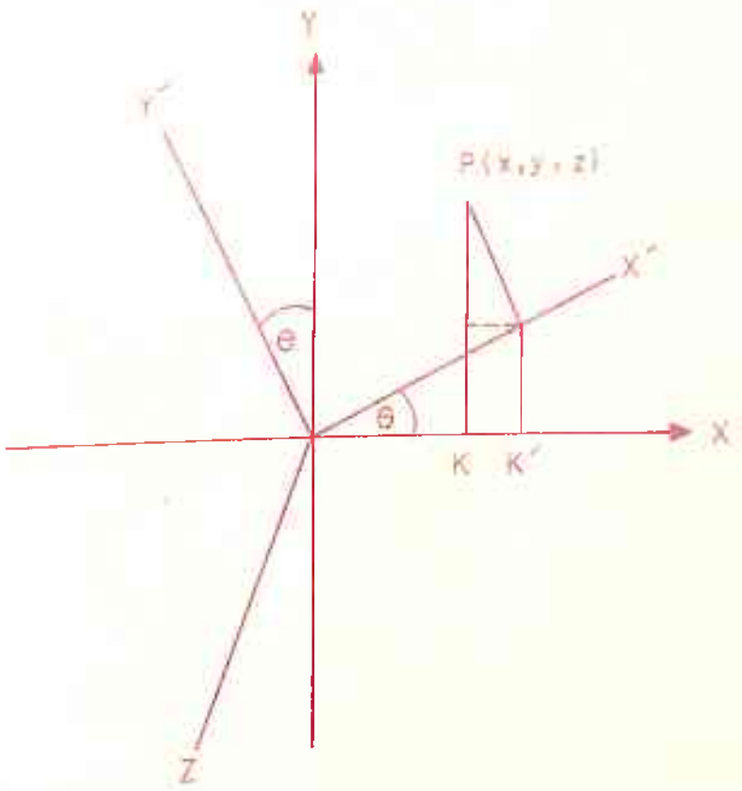

FIG.25 SHOWS CARTESIAN COORDINATE SYSTEM AFTER A ROTATION THROUGH ANGLE θ ABOUT Z-AXIS.

after rotation through 2π, which is identity transformation and is denoted by E having its matrix as

$$E = \begin{bmatrix} 1 & 0 & 0 \\ 0 & 1 & 0 \\ 0 & 0 & 1 \end{bmatrix}$$

The rotation operation through $\frac{2\pi}{n}$ angle is denoted by the symbol C_n. If $n=2$, the angle through which the body is rotated is $\frac{2\pi}{2} = \pi$ and the operation will be C_2. Similarly, for $n=3$ the operation is represented as C_3. The matrix forms for C_2 and C_3 operations can be obtained from the equation (2) after substituting $\theta = \frac{2\pi}{2}$ and $\theta = \frac{2\pi}{3}$ respectively as follows:

$C_2 \equiv$ (rotation about z-axis)

$$\begin{bmatrix} \cos\pi & -\sin\pi & 0 \\ \sin\pi & \cos\pi & 0 \\ 0 & 0 & 1 \end{bmatrix}$$

$$\equiv \begin{bmatrix} -1 & 0 & 0 \\ 0 & -1 & 0 \\ 0 & 0 & 1 \end{bmatrix}$$

$C_3 \equiv$ (rotation about z-axis)

$$\begin{bmatrix} \cos\frac{2\pi}{3} & -\sin\frac{2\pi}{3} & 0 \\ \sin\frac{2\pi}{3} & \cos\frac{2\pi}{3} & 0 \\ 0 & 0 & 1 \end{bmatrix}$$

$$\equiv \begin{bmatrix} -1/2 & -\sqrt{3}/2 & 0 \\ \sqrt{3}/2 & -1/2 & 0 \\ 0 & 0 & 1 \end{bmatrix}$$

C_a is the operation which gives a rotation of π about a-axis and C_b is the rotation of π about b-axis such that $C_2 C_a = C_b$. The rotation operations C_a and C_b are shown in Figure 26.

Thus C_a and C_b can be represented in the matrix form as

$$C_a \equiv \begin{bmatrix} 1 & 0 & 0 \\ 0 & -1 & 0 \\ 0 & 0 & -1 \end{bmatrix}, \qquad C_b \equiv \begin{bmatrix} -1 & 0 & 0 \\ 0 & 1 & 0 \\ 0 & 0 & -1 \end{bmatrix}$$

$$C_c \equiv \begin{bmatrix} -1 & 0 & 0 \\ 0 & -1 & 0 \\ 0 & 0 & 1 \end{bmatrix}$$

$S_4 = C_4 \sigma$; where σ reflection in a perpendicular plane C_4 is the operation in which a rotation through angle $\frac{2\pi}{4}$ will be made about an axis. Therefore, S_4 is called rotation-reflection operation and can be represented in matrix form as

$$S_4 \equiv \begin{bmatrix} 0 & -1 & 0 \\ 1 & 0 & 0 \\ 0 & 0 & -1 \end{bmatrix}$$

σ_v is the reflection in x-z plane and its matrix form is given by

$$\sigma_v \equiv \begin{bmatrix} 1 & 0 & 0 \\ 0 & -1 & 0 \\ 0 & 0 & 1 \end{bmatrix}$$

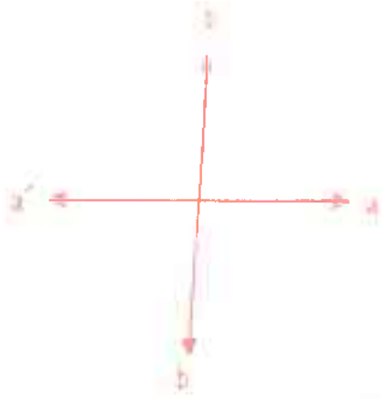

(a) ORIGINAL POSITION OF AXES

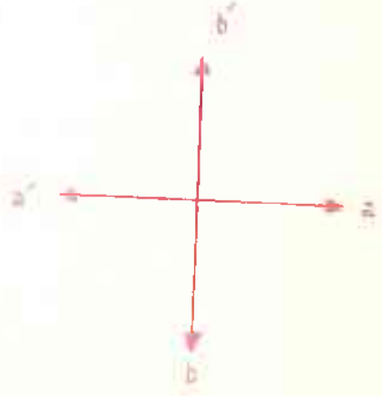

(b) AFTER THE APPLICATION C
OPERATION C_a OVER (a)

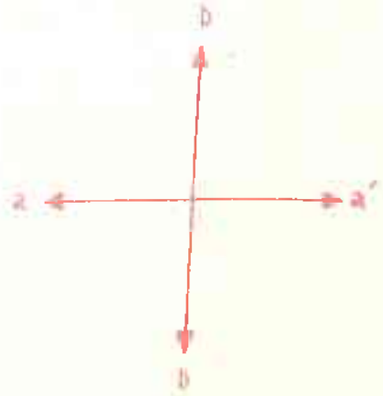

(c) APPLICATION OF C_2 OPERATION; THIS IS EXACTLY LIKE APPLYING C_b TO (a)

FIG.26 SHOWS C_a AND C_b ROTATION OPERATIONS.

Similarly, σ_v' and σ_v'' being the reflections in the y-z plane and x-y plane respectively, have the matrix forms as

$$\sigma_v' \equiv \begin{bmatrix} -1 & 0 & 0 \\ 0 & 1 & 0 \\ 0 & 0 & 1 \end{bmatrix}, \qquad \sigma_v'' \equiv \begin{bmatrix} 1 & 0 & 0 \\ 0 & 1 & 0 \\ 0 & 0 & -1 \end{bmatrix}$$

÷÷:÷:÷÷:÷÷

REFERENCES

(1) W. Kaiser and C.G.B. Garret: Phys. Rev. Lett. 7, 229 (1961)

(2) I.D. Abella: Phys. Rev. Lett. 9, 453 (1962)

(3) S. Singh and L.T. Bradley: Phys. Rev. Lett. 12, 612 (1964)

(4) D.A. Kleinman: Phys. Rev. 125, 87 (1962)

(5) P.A. Franken, A.E. Hill, C.W. Peters and G. Weinrich: Phys. Rev. Lett. 7, 118 (1961)

(6) R.W. Hellwarth: "Advances in Quantum Electronics" (Columoia University Press, New York, 1961), p. 334.

(7) F.J. McClung and R.W. Hellwarth: J. Appl. Phys. 33, 828 (1962)

(8) R.J. Collins and P. Kisliuk: J. Appl. Phys. 33, 2009 (1962)

(9) A.J. DeMaria, R. Gagosz, and G. Barnard: J. Appl. Phys. 34, 453 (1963)

(10) Technical report on "Laser Research in India" dated May 3, 1966, from Optical Maser Laboratory, I.I.T., Kanpur (India); also refer to Dheer, Madhavan and Jaseja: Appl. Phys. Lett. 8, 225 (1966)

(11) T.S. Jaseja, P.C. Pande, V. Parkash and B. Kumar: IEEE JQE 7, 537 (1971)

(12) M. Göppert-Mayer: Ann. Physik. 9, 847 (1931)

(13) Refer to D.S. McClure: "Solid State Physics" edited by F. Seitz and D. Turnbull, Eds. (Academic Press, Inc., New York, 1959), Vol. 8, p. 1; H.C. Wolf in, ibid: Vol. 9, p. 1.

(14) R.M. Hochstrasser: Rev. Mod. Phys. 34, 531 (1962)

(15) W.L. Peticola, J.P. Goldsborough, and K.B. Rieckhoff: Phys. Rev. Lett. 10, 43 (1963); W.L. Peticola and K.B. Rieckhoff; J. Chem. Phys. 39, 1347 (1963)

(16) S. Singh and B.P. Stoicheff: J. Chem. Phys. 38, 2032 (1963)

(17) R.S. Kepler, J.C. Caris, P. Avakian and E. Abramson: Phys. Rev. Lett. 10, 400 (1963)

(18) J.L. Hall, D.A. Jennings, and R.M. McClintok: Phys. Rev. Lett. 11, 364 (1963)

(19) S. Singh, W.J. Jones, W. Siebrand, B.P. Stoicheff, and W.G. Scneider: J. Chem. Phys. 42, 330 (1965)

(20) L.I. Schiff: "Quantum Mechanics" (third edition), (McGraw-Hill, 1968, p. 282

(21) J.W. Sidman: Phys. Rev. 102, 96 (1956)

(22) J. Ferguson: J. Chem. Phys. 28, 765 (1958)

(23) S.C. Ganguly and N.K. Choudhury: J. Chem. Phys. 21, 554 (1953)

(24) N.S. Ham and K. Ruedenberg: J. Chem. Phys. 25, 13 (1956)

(25) D.S. McClure and S. Schnepp: J. Chem. Phys. 23, 1575 (1955)

(26) M. Goreimov and K. Shebaldas: J. Phys. USSR 7, 168 (1943)

(27) P.A. Franken and J.F. Ward: Rev. Mod. Phys. 35, 23 (1963)

(28) "Group Theory", M. Hamermesh p. 32

(29) "Quantum Chemistry", Iyring, Kimbel and Walter p. 381.

(30) R.W. Terhune, P.D. Maker and C.M. Savage: Phys. Rev. Lett. 8, 404 (1962)

(31) J.A. Giordmaine: Phys. Rev. Lett. 8, 19 (1962)

(32) P.D. Maker, R.W. Terhune, M. Nisenoff, and C.M. Savage: Phys. Rev. Lett. 8, 21 (1962)

(33) "Lasers", A.K. Levine Vol. 2 p. 329

(34) G. Eckhardt, R.W. Hellwarth, F.J. McClung, S.E. Schwarz, D. Weiner and E.J. Woodbury: Phys. Rev. Lett. 9, 455 (1962)

(35) R.W. Terhune; Bull. Am. Phys. Soc., 118, 359 (1963); Solid State Design, 4, 38 (1963)

(36) B.P. Stoicheff: Phys. Lett. 7, 186 (1963); "Symposium on molecular structure and spectroscopy", Ohio State University (June 1963)

(37) H.J. Zeiger, P.E. Tannelwald, S. Kern and R. Harendeen: Phys. Rev. Lett. 11, 419 (1963)

(38) F.J. McClung, R.J. Wagner and D. Weiner: Phys. Rev. Lett. 15, 96 (1965)

(39) M.K. Dheer, D. Madhavan and T.S. Jaseja: Appl. Phys. Lett. 8, 225 (1966)

(40) T.S. Jaseja, M.K. Dheer and D. Madhavan: J. Appl. Phys. 37, 4995 (1966)

(41) Ved Parkash, M.K. Dheer and T.S. Jaseja: Phys. Lett. 29A, 220 (1969)

(42) T.S. Jaseja, Ved Parkash, M.K. Dheer and S.C. Sethi: J. Chem. Phys. 54, 1419 (1971)

(43) Ved Parkash and T.S. Jaseja: J. Appl. Phys. 42, 404 (1971)

(44) Ved Parkash, S.C. Sethi, M.K. Dheer and T.S. Jaseja: Ind. J. Pure and Appl. Phys. 9, 95 (1971)

(45) R.W. Minck, R.W. Terhune and W.G. Rado: Appl. Phys. Lett. 3, 181 (1963)

(46) R.Y. Chiao and B.P. Stoicheff: Phys. Rev. Lett. 12, 290 (1964)

(47) A. Javan: Bull. Am. Phys. Soc. 3, 213 (1956); Phys. Rev. 107, 1579 (1957); Phys. et. Rad. 12, 806 (1958)

(48) E. Garmire, F. Pandarcse and C.H. Townes: Phys. Rev. Lett. 11, 160 (1963)

(49) R.Y. Chiao, E. Garmire and C.H. Townes: Proc. of the International School of Physics, E. Fermi, Course XXXI Academic Press, New York (1964), p. 306

(50) A. Javan: Proc. of the International School of Physics, E. Fermi, Course XXXI Academic Press, New York, p. 284

(51) Y.R. Shen and N. Bloembergen: Phys. Rev. 137, A1787 (1965)

(52) R.W. Hallwarth; Appl. Opt. 2, 847 (1963)